

See discussions, stats, and author profiles for this publication at: <https://www.researchgate.net/publication/270963132>

# Homodimeric anoctamin-1, but not homodimeric anoctamin-6, is activated by calcium increases mediated by the P2Y1 and P2X7 receptors

ARTICLE *in* PFLÜGERS ARCHIV - EUROPEAN JOURNAL OF PHYSIOLOGY · JANUARY 2015

Impact Factor: 4.1 · DOI: 10.1007/s00424-015-1687-3 · Source: PubMed

---

READS

16

## 7 AUTHORS, INCLUDING:



Michaela Stolz

University Hospital RWTH Aachen

2 PUBLICATIONS 0 CITATIONS

[SEE PROFILE](#)



Manuela Klapperstück

Martin Luther University Halle-Wittenberg

28 PUBLICATIONS 400 CITATIONS

[SEE PROFILE](#)



Günther Schmalzing

RWTH Aachen University

117 PUBLICATIONS 3,961 CITATIONS

[SEE PROFILE](#)



Fritz Markwardt

Martin Luther University Halle-Wittenberg

80 PUBLICATIONS 1,302 CITATIONS

[SEE PROFILE](#)

# Homodimeric anoctamin-1, but not homodimeric anoctamin-6, is activated by calcium increases mediated by the P2Y1 and P2X7 receptors

Michaela Stolz · Manuela Klapperstück ·  
Thomas Kendzierski · Silvia Detro-dassen ·  
Anna Panning · Günther Schmalzing · Fritz Markwardt

Received: 22 July 2014 / Revised: 23 December 2014 / Accepted: 6 January 2015  
© Springer-Verlag Berlin Heidelberg 2015

**Abstract** The P2X7 receptor (P2X7R) is a ligand-gated ion channel that conducts  $\text{Na}^+$ ,  $\text{K}^+$ , and  $\text{Ca}^{2+}$  when activated by extracellular ATP. In various cell types, such as secretory epithelia, the P2X7R is co-expressed with  $\text{Ca}^{2+}$ -dependent  $\text{Cl}^-$  channels of the TMEM16/anoctamin family. Here, we studied whether the P2X7R and TMEM16A/anoctamin-1 (Ano1) or TMEM16F/anoctamin-6 (Ano6) interact functionally and physically, using oocytes of *Xenopus laevis* and *Ambystoma mexicanum* (Axolotl) for heterologous expression. As a control, we co-expressed anoctamin-1 with the P2Y1 receptor (P2Y1R), which induces the release of  $\text{Ca}^{2+}$  from intracellular stores via activating phospholipase C through coupling to G $\alpha$ q. We found that co-expression of anoctamin-1 with the P2Y1R resulted in a small transient increase in  $\text{Cl}^-$  conductance in response to ATP. Co-expression of anoctamin-1 with the P2X7R resulted in a large sustained increase in  $\text{Cl}^-$  conductance via  $\text{Ca}^{2+}$  influx through the ATP-opened P2X7R in *Xenopus* and in Axolotl oocytes, which lack endogenous  $\text{Ca}^{2+}$ -dependent  $\text{Cl}^-$  channels. P2Y1R- or P2X7R-mediated stimulation of Ano1 was primarily functional, as demonstrated by the absence of a physically stable interaction between Ano1 and the P2X7R. In the pancreatic cell line AsPC-1, we found the same functional  $\text{Ca}^{2+}$ -

dependent interaction of P2X7R and Ano1. The P2X7R-mediated sustained activation of Ano1 may be physiologically relevant to the time course of stimulus-secretion coupling in secretory epithelia. No such increase in  $\text{Cl}^-$  conductance could be elicited by activating the P2X7 receptor in either *Xenopus* oocytes or Axolotl oocytes co-expressing Ano6. The lack of function of Ano6 can, at least in part, be explained by its poor cell-surface expression, resulting from a relatively inefficient exit of the homodimeric Ano6 from the endoplasmic reticulum.

**Keywords** Anoctamin-1 · Anoctamin-6 · P2X7 receptor · Quaternary structure · Intracellular  $\text{Ca}^{2+}$

## Introduction

According to their relatedness in terms of sequences, structures, and signal transduction mechanisms, the purinergic P2 receptors fall naturally into two classes: the seven-member family of P2X receptors (P2X1R-P2X7R) and the eight-member family of P2Y receptors (P2Y1R, P2Y2R, P2Y4R, P2Y6R, P2Y11R, P2Y12, P2Y13, and P2Y14), which function as ligand-gated cation channels and G protein-coupled receptors, respectively [58, 64, 88]. P2X and P2Y receptors are ubiquitously distributed throughout the body. Within the P2X family, P2X7R is highly expressed on cells of the immune and inflammatory system [18] and in the secretory epithelia [59]. In the immune system, ATP released from hypoxic, inflammatory, or necrotic tissue acts as a danger signal by activating P2X7R [18]. The activation of P2X7R has immunomodulatory functions and contributes to the release of proinflammatory cytokines such as interleukin-1 $\beta$  [18], interleukin-6 [79], and interleukin-18 [52]. In epithelia,

Günther Schmalzing and Fritz Markwardt share senior authorship.

**Electronic supplementary material** The online version of this article (doi:10.1007/s00424-015-1687-3) contains supplementary material, which is available to authorized users.

M. Stolz · S. Detro-dassen · A. Panning · G. Schmalzing  
Molecular Pharmacology, RWTH Aachen University,  
Wendlingweg 2, D-52074 Aachen, Germany

M. Klapperstück · T. Kendzierski · F. Markwardt (✉)  
Julius-Bernstein-Institute for Physiology, Martin-Luther-University  
Halle-Wittenberg, Magdeburger Str. 6, D-06097 Halle/Saale,  
Germany  
e-mail: fritz.markwardt@medizin.uni-halle.de

P2X7R is involved in the control of fluid secretion from exocrine glands [35, 53].

The cellular effects of P2X7R activation are at least partly mediated by the influx of  $\text{Ca}^{2+}$  [2] and  $\text{Na}^+$  [48] and the resulting efflux of  $\text{K}^+$  [18]. A P2X7R-mediated increase in anion conductance has also been observed in several studies [5, 6, 16, 59]. One possible explanation for this finding is that anions travel through P2X7R as a result of the loss of cation selectivity associated with the dilation of the P2X7R channel pore [15, 20, 62, 67, 81] observed after the prolonged application of high concentrations of ATP [11, 58]. An alternative possibility considered here is that the stimulation of P2X7R secondarily activates specific anion channels, either through increasing cytosolic  $\text{Ca}^{2+}$  or via direct interaction of P2X7R with a distinct channel protein. There are precedents for both possibilities in the literature, including the indirect activation of a large nonselective cation channel via a P2X7R-mediated increase in the intracellular  $\text{Ca}^{2+}$  concentration ( $[\text{Ca}^{2+}]_i$ ) [25] and direct protein-protein interactions of P2X7R with various cellular proteins [37, 38, 61, 92]. In particular, the long C-terminal tail of hP2X7R has been suggested to serve as a scaffold for interactions with other proteins [7, 8]. Here, we investigated whether the  $\text{Ca}^{2+}$ -activated chloride channels (CaCCs) TMEM16A/Ano1 (Ano1) [14, 75] and TMEM16F/Ano6 (Ano6) [27, 44, 82] are activated secondary to the activation of P2X7R, which is known to mediate  $\text{Ca}^{2+}$  influx and the associated increase in  $[\text{Ca}^{2+}]_i$  [4, 22]. Partial results of this work were presented in a poster at the 5th Joint Italian-German Purine Club Meeting in Rimini (Italy) in 2013 and published in abstract form at [www.unibo.it/meeting/purineclub2013/programme](http://www.unibo.it/meeting/purineclub2013/programme).

## Materials and methods

**Reagents** Unless otherwise stated, chemicals and molecular biology reagents were purchased from Sigma (Sigma-Aldrich, Taufkirchen, Germany), Merck (Darmstadt, Germany), and New England Biolabs (Schwalbach, Germany).

**Individual expression and co-expression of P2X7, P2Y1, Ano1, and Ano6 in oocytes of *Xenopus laevis* and Axolotl** The oocyte expression plasmids encoding the human P2X7R (hP2X7R) subunit (GenBank Y09561) and the mouse mTMEM16A(a) (mAno1) subunit (GenBank NM\_178642.4) have been previously described [24, 40, 65]. cDNAs comprising the entire coding region of mouse P2Y1R (mP2Y1R, GenBank NM\_008772.5) [86], human Ano6 (hAno6, GenBank NM\_001025356.2) [82], and mouse Ano6 (mAno6, GenBank NM\_175344.4) [82] were obtained from Source BioScience (Nottingham, UK) and subcloned via PCR from the vectors pBluescriptR and pCMV-SPORT into a Gateway-modified version of the oocyte expression vector

pNKS2 [29]. Oocyte expression plasmids encoding the  $\alpha 1$  subunit of the human glycine-activated receptor (GlyR) and the mouse serotonin type 3 receptor (5HT<sub>3</sub>R) have been described previously [31, 57].

The plasmids were linearized downstream of the vector-provided polyA tail and transcribed with SP6 RNA polymerase into capped and polyadenylated cRNA, as previously described [40]. The sole exception was the use of the “anti-reverse” cap analog ARCA ( $m^{7,3'-O}\text{GpppG}$ , Jena Bioscience, Germany, product NU-855), which can be incorporated only in the correct orientation at the 5' end of the cRNA and should therefore increase translation efficiency [33].

*X. laevis* oocytes were defolliculated through treatment with collagenase (NB 4G, Serva, Heidelberg, Germany). Oocytes in stages V–VI were individually injected with 25–50 ng of cRNA, except for the hP2X7R cRNA, for which only 1–5 ng was injected into the oocytes to be used in electrophysiological experiments to keep the maximum ATP-elicited current amplitudes below 5  $\mu\text{A}$ . The oocytes were incubated at 19 °C in sterilized frog Ringer's solution (Mg/Ca-ORI: 100 mM NaCl, 2.5 mM KCl, 1 mM MgCl<sub>2</sub>, 1 mM CaCl<sub>2</sub>, and 10 mM HEPES, pH 7.4) supplemented either with penicillin (100 U/ml) and streptomycin (100  $\mu\text{g}/\text{ml}$ ) or solely with gentamycin (50  $\mu\text{g}/\text{ml}$ ) [26]. The procedures followed for the maintenance and surgery of the frogs were approved by the local animal welfare committees (Magdeburg, Germany, reference no. 53a-42502/2-173, and Düsseldorf, Germany, reference no. 8.87-51.05.20.10.131 for experiments performed in Halle and Aachen, respectively), in compliance with EC Directive 86/609/EEC for animal experiments.

Collagenase-defolliculated Axolotl oocytes were purchased from EcoCyte Bioscience (Castrop-Rauxel, Germany). We handled the Axolotl oocytes exactly as the *X. laevis* oocytes except that we increased the amount of injected cRNA two- to eightfold to account for the about eightfold larger volume of the Axolotl oocytes.

**Two-electrode voltage-clamp electrophysiology** The electrophysiological experiments were performed at room temperature (~22 °C). Rapid, reproducible solution exchange was accomplished using a small tube-like chamber (0.1 ml) combined with fast superfusion (75  $\mu\text{l}/\text{s}$ ). A set of computer-controlled magnetic valves combined with a modified U-tube technique permitted the bathing solutions to be changed in less than 1 s [40]. Whole-cell membrane currents were recorded via the two-electrode voltage-clamp (TEVC) method using 3 M KCl-filled microelectrodes (resistances 0.8–1.2 MΩ). In experiments in which extracellular Cl<sup>−</sup> was substituted with glutamate<sup>−</sup>, the reference electrodes were connected to the bath by 3 M KCl-agar bridges. The remaining diffusion potentials in the glutamate<sup>−</sup>-based extracellular solutions were approximated as -10 mV based on a previously described protocol [43] and were subtracted accordingly. The

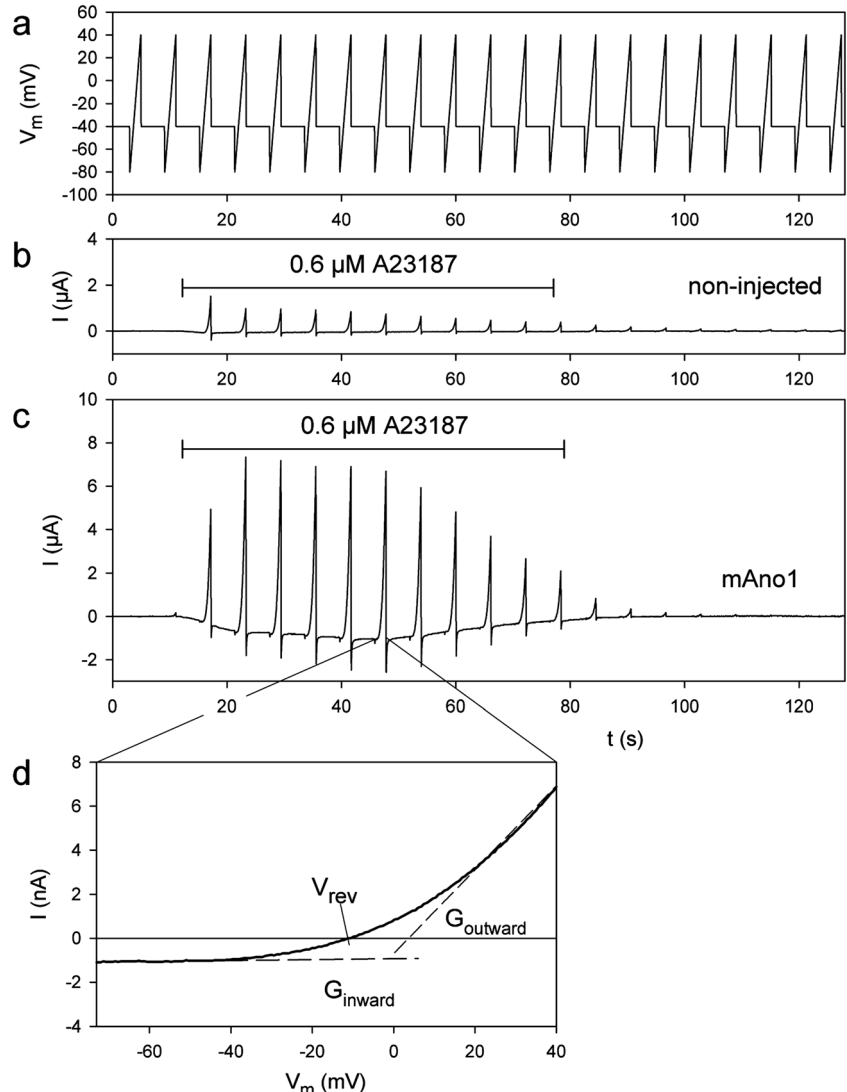
currents were recorded and filtered at 100 Hz using an oocyte clamp amplifier (OC-725C, Hamden, USA) and sampled at 85 Hz. The data were stored and analyzed on a personal computer using software written in our department (Superpatch 2000, SP-Analyzer by T. Böhm).

Two days after cRNA injection, individual oocytes were superfused with Mg/Ca-ORi and impaled with the voltage-clamp electrodes. To record the ionic currents in the absence and presence of external  $\text{Ca}^{2+}$ , the superfusion medium was switched between the following three ORi-based media (ORi: 100 mM NaCl, 2.5 mM KCl, 5 mM Hepes, pH 7.4), all of which lacked added  $\text{Mg}^{2+}$  to prevent the complexation of the P2X7R agonist ATP $^{4-}$  with  $\text{Mg}^{2+}$ : (i) Ca-ORi containing 1 mM  $\text{CaCl}_2$ , (ii) Ca-ORi-Flu containing 1 mM  $\text{CaCl}_2$  and 0.1 mM flufenamic acid, and (iii) EGTA-ORi-Flu without added  $\text{CaCl}_2$ , containing 1 mM EGTA and 0.1 mM flufenamic acid. As previously reported [40], the rationale for including flufenamic acid was to suppress the large inward conductance

that consistently develops in the virtual absence of both the  $\text{Mg}^{2+}$  and  $\text{Ca}^{2+}$  divalent ions. Of note, comparative recordings obtained from oocytes in Ca-ORi and Ca-ORi-Flu allowed detection of the conductance changes, if any, produced by flufenamic acid under conditions in which the development of the flufenamic acid-sensitive large inward conductance was prevented by the presence of 1 mM  $\text{CaCl}_2$  in the bath. Because all current recordings were performed in  $\text{Mg}^{2+}$ -free media, only the potential for  $\text{Ca}^{2+}$  to diminish  $\text{ATP}^{4-}$  by forming a  $\text{Ca}-\text{ATP}$  complex had to be considered. This possibility was accounted for by calculating the absolute concentrations of  $\text{CaCl}_2$  and ATP needed to achieve the indicated  $\text{ATP}^{4-}$  concentrations with 1 mM free  $\text{Ca}^{2+}$  following published guidelines [76].

To suppress the activation of  $\text{Ca}^{2+}_{\text{i}}$ -dependent currents, in some of the experiments, 2 to 4 h before the currents were recorded, the oocytes were injected with 100 mM BAPTA (23 nl/oocyte) to a concentration of  $\approx 5$  mM, calculated by

**Fig. 1** Effect of A23187 on voltage ramp-evoked current traces in native and mAno1-expressing oocytes. **a** The voltage ramp protocol used to probe the current–voltage relationship over time. **b, c:** Time course of ramp currents before, during, and after the superfusion of native or mAno1-expressing oocytes in Ca-ORi with the  $\text{Ca}^{2+}$  ionophore A23187 for the time indicated by the horizontal bar. **d:** Current–voltage (IV) relationship obtained by plotting the ramp current amplitudes from **c** versus the applied membrane potential, as indicated. The inwardly and outwardly directed conductances  $G_{\text{outward}}$  and  $G_{\text{inward}}$ , respectively, were taken as the slopes of the I–V curve in the voltage ranges of  $-75$  to  $-40$  mV and  $+20$  to  $+40$  mV, respectively. The reversal potential ( $V_{\text{rev}}$ ) is given by the voltage intercept at zero current



assuming 0.5  $\mu$ l of intracellular water per oocyte. The agonists and antagonists were diluted in the appropriate ORi solution, as indicated in the figures. The  $\text{Ca}^{2+}$  ionophore A23187 was diluted from a 5 mM stock in DMSO, first to 1.2  $\mu$ M in the appropriate ORi solution and then immediately to 0.6  $\mu$ M by mixing an aliquot with an equal volume of ORi in the oocyte superfusion chamber. The superfusion was transiently stopped to allow a contact time with A23187 of 60 s. A23187 and ATP were applied only once per oocyte.

Ramp currents were measured by applying a 2-s-duration linear ramp from -80 to +40 mV every 6 s. Between the ramps, the holding potential was maintained at -40 mV (see Fig. 1a). The currents induced by ATP or A23187 were calculated as the difference between the ramp currents before and during the application of ATP or A23187.

**Whole-cell voltage clamp of AsPC-1 cells** The human pancreatic adenocarcinoma cell line AsPC-1 (ATCC® CRL-1682) was kindly provided by Prof. Dr. Barbara Seliger (Institute of Medical Immunology, Martin-Luther-University Halle). The cells were grown on poly-L-lysine-coated 5-mm diameter coverslips in RPMI medium supplemented with 10 % heat-inactivated fetal calf serum, 100 U/ml penicillin, 100  $\mu$ g/ml streptomycin, and 0.25  $\mu$ g/ml of amphotericin B. Voltage clamp of the cell membrane was performed as previously described [10, 48]. The patch pipettes were filled with 120 mM Na-aspartate, 10 mM Glucose, 0.2 mM EGTA, 10 mM Hepes, 5.5 mM MgCl<sub>2</sub>, and 5 mM NaATP, pH 7.2. To suppress the activation of  $[\text{Ca}^{2+}]_i$ -dependent ion currents, 3 mM EGTA and 3 mM BAPTA were used instead of 0.2 mM EGTA. After transferring a coverslip to the recording chamber, the cells were superfused with bathing solution consisting of 140 mM NaCl, 5.4 mM KCl, 0.5 mM MgCl<sub>2</sub>, 1 mM CaCl<sub>2</sub>, 10 mM glucose, and 10 mM Hepes, pH 7.4. For measurement of ion currents, the bathing solution was replaced by an extracellular solution containing 140 mM NaCl or TrisCl, 10 mM glucose, 10 mM Hepes, and 0.5 mM CaCl<sub>2</sub>, pH 7.4. Ramp currents were measured by application of 0.5 s lasting linear ramps from -80 to +40 mV every 1 s. The holding potential was maintained at -40 mV (see Fig. 12). For activation of  $[\text{Ca}^{2+}]_i$ -dependent currents, 1  $\mu$ M A23187 or 0.1 mM BzATP<sup>4-</sup> dissolved in the extracellular solution were applied via an U-tube for 20 s.

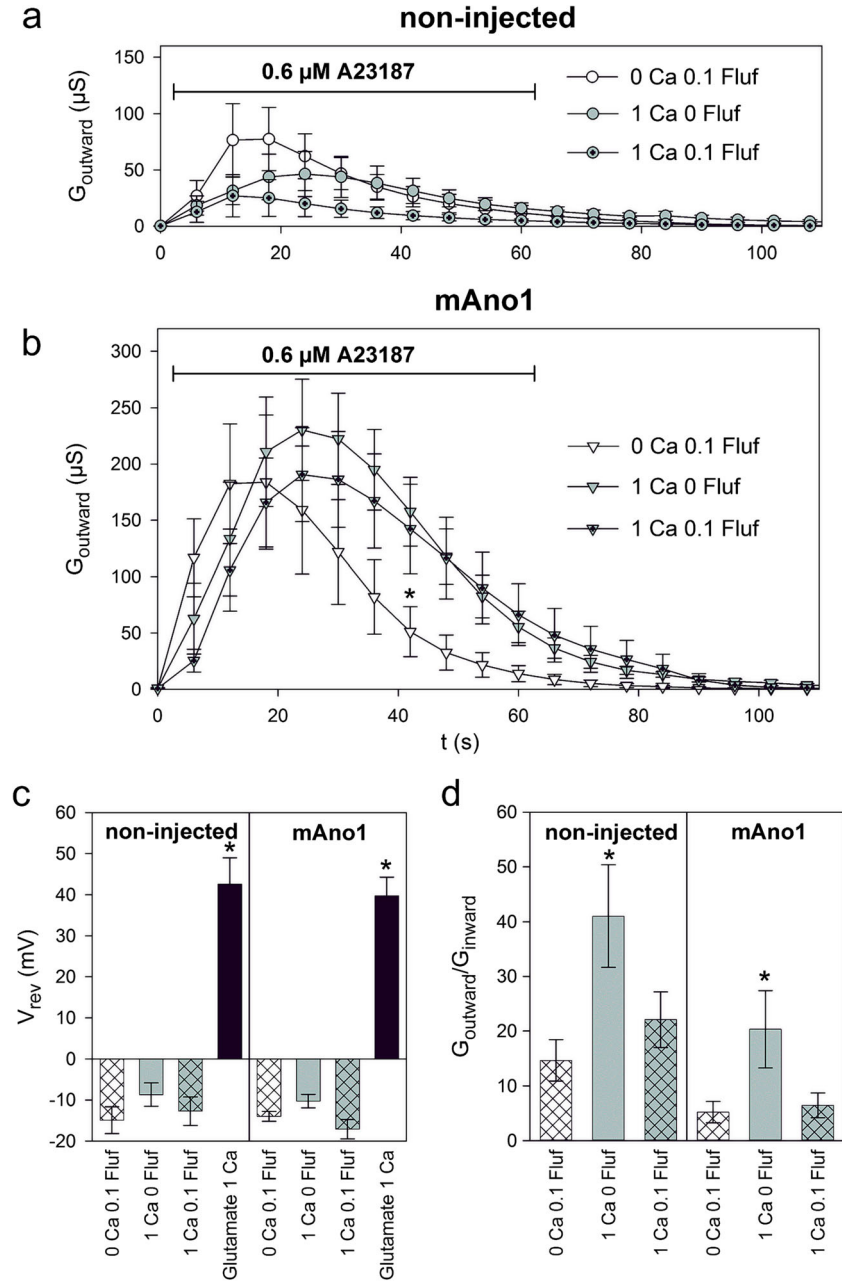
**Protein purification and detection** The cRNA-injected oocytes were metabolically labeled at 19 °C via overnight incubation with L-[<sup>35</sup>S]-methionine (>40 TBq/mmol; PerkinElmer Life Sciences, Überlingen, Germany) in sterile ORi. After an additional 24 h chase period at 19 °C, the surface of the intact oocytes was labeled with an amine-reactive, membrane-impermeable fluorescent

dye (Cy5-NHS ester GE Healthcare or IR dye 800CW NHS ester, LI-COR, Bad Homburg, Germany) immediately prior to protein extraction with the detergent digitonin (Calbiochem, Darmstadt, Germany), as previously described [7]. Proteins tagged with a His-tag or a StrepII-tag were purified via non-denaturing affinity chromatography using nickel-nitriloacetic acid (Ni-NTA) agarose (QIAGEN, Hilden, Germany) or Strep-Tactin® Sepharose (IBA, Göttingen, Germany), as appropriate [7]. The proteins were released from the Ni-NTA agarose or Strep-Tactin Sepharose using a non-denaturing buffer consisting of 1 % (w/v) digitonin in 250 mM imidazole/HCl, pH 7.6, either alone or supplemented with 10 mM biotin, respectively. Alternatively, hP2X7R was purified as previously described [72] via non-denaturing immunoprecipitation, using a monoclonal antibody against the hP2X7R receptor [13] and protein A Sepharose CL-4B (GE Healthcare, Freiburg, Germany). The antibody-bound hP2X7R and any potentially associated proteins were released from the protein A Sepharose through two sequential 15-min incubations at 56 °C, each using 50  $\mu$ l of colorless sodium dodecyl sulfate polyacrylamide gel electrophoresis (SDS-PAGE) sample buffer.

The proteins purified by either method were resolved via denaturing SDS-urea-PAGE under non-reducing and reducing (20 mM DTT) conditions. To determine their glycosylation state, the proteins were treated prior to SDS-PAGE with either endoglycosidase H (EndoH) or PNGase F (New England Biolabs, Beverly, MA) for 4 h in reducing SDS sample buffer supplemented with 1 % (w/v) octylglucoside (Anatrace, Maumee, USA) to counteract the SDS-mediated inactivation of PNGase F. A bromophenol blue-free and therefore colorless SDS sample buffer was used throughout the SDS-PAGE procedure to prevent blue staining of the SDS-PAGE gel that might interfere with fluorescence detection.

In some of the experiments, the proteins purified via Ni-NTA chromatography were additionally resolved in their non-denatured and partially SDS-denatured states through blue native PAGE (BN-PAGE) to display their oligomeric state, as previously described [24, 34]. As molecular mass markers for BN-PAGE, we co-analyzed His-tagged versions of the oocyte-expressed homopentameric ligand-gated ion channels GlyR or SHT<sub>3</sub>R, which were in each experiment freshly purified from oocytes of *X. laevis* or Axolotl, as indicated. When PAGE was complete, the gels were scanned wet on an appropriate fluorescence scanner (Typhoon, GE Healthcare or Odyssey Infrared Imager LI-COR, Bad Homburg, Germany) to visualize the fluorescently labeled plasma membrane-bound proteins. The PAGE gels were subsequently dried for additional detection of <sup>35</sup>S

**Fig. 2** Time course of the conductance changes induced by A23187 in native and mAno1-expressing oocytes. **a, b** The data were obtained following the protocol shown in Fig. 1 and represent the means $\pm$ SEM of 6–7 oocytes each. The outward conductances were determined in **a** native oocytes and **b** mAno1-expressing oocytes in response to a 60-s application of A23187 (horizontal bar) in the indicated ORi solution. The ramp currents recorded before the application of A23187 were subtracted. **c, d** The bars represent the means $\pm$ SEM (from 6–7 oocytes each) of  $V_{rev}$  and the outward rectification index ( $G_{outward}/G_{inward}$ ) calculated 20 s after the application of A23187. The same protocol was used to measure  $V_{rev}$  in Ca-ORi-Glu, in which  $Cl^-$  was replaced by glutamate $^-$  (“Glutamate 1 Ca” in **c**). Significant differences between the means are indicated by asterisks. “0 Ca 0.1 Fluf” = EGTA-ORi-Flu without added  $CaCl_2$ , containing 1 mM EGTA and 0.1 mM flufenamic acid, “1 Ca 0 Fluf” = Ca-ORi containing 1 mM  $CaCl_2$  and no flufenamic acid; “1 Ca 0.1 Fluf” = Ca-ORi-Flu containing 1 mM  $CaCl_2$  and 0.1 mM flufenamic acid



incorporation using a PhosphorImager (Storm 820, GE Healthcare).

**Data analysis and presentation** Non-linear approximations and the presentation of data were accomplished using the program SigmaPlot (Systat Software Inc.). Averaged data are presented as the means $\pm$ SEM. Statistical data were analyzed via one-way ANOVA. The statistical significance of the differences between means was tested using multiple *t* tests (Bonferroni) with the SigmaPlot program. Significance was set at  $p<0.05$ . Images of the PAGE gels were prepared using ImageQuant TL software version 7.0 (GE Healthcare

Biosciences), Adobe Photoshop CS 8.0, and Microsoft PowerPoint 2000, as previously described [24].

## Results

**Activation of Ano1 by the Ca ionophore A23187** Typical TEVC current recordings from native *X. laevis* oocytes and mAno1-expressing oocytes are shown in Fig. 1. In the presence of the  $Ca^{2+}$  ionophore A23187, the application of voltage-ramp pulses ranging from  $-80$  mV to  $+40$  mV

(Fig. 1a) to native *X. laevis* oocytes revealed small outward currents that decreased over time, despite the continued presence of A23187 (Fig. 1b). We applied ramp pulses rather than square pulses to evaluate the steady-state current–voltage (IV) relationship in a time period that was sufficiently short to avoid marked conductance changes [46]. Similar, but significantly larger ramp currents were recorded when the same protocol was applied to oocytes expressing mAno1; these ramp currents also became smaller over time in the continued presence of A23187 (Fig. 1c). The mAno1-mediated current at the holding potential of  $-40$  mV between voltage ramps is reflected by the inward shift of the current relative to the baseline (Fig. 1c). Plotting the recorded currents against the ramp-pulse voltage revealed an outwardly rectifying current–voltage relationship with a reversal potential ( $V_{rev}$ ) of approximately  $-10$  mV (Fig. 1d). Both the strong outward rectification and the  $V_{rev}$  of  $-10$  mV are representative of CaCCs [45, 75].

For statistical analysis of the experimental data, the slopes of the recorded voltage-dependent ramp currents were transformed to conductances (G) and plotted against time (Fig. 2a, b). The curves show that A23187 induced an increase in outward conductance in both native oocytes (Fig. 2a) and mAno1-expressing oocytes (Fig. 2b). The conductance started to decline over time already in the presence of A23187 (Fig. 2a, b). In the native oocytes, the increase in conductance was statistically unaffected by the absence or presence of  $\text{Ca}^{2+}$  in the bath, suggesting that the A23187-induced release of  $\text{Ca}^{2+}$  from intracellular stores was sufficient to fully activate the conductance (Fig. 2a). In contrast, in the mAno1-expressing oocytes, the conductance was greater when  $\text{Ca}^{2+}$  was present in the bath, suggesting that an A23187-induced  $\text{Ca}^{2+}$  influx from the extracellular medium contributed to the activation of the mAno1-dependent currents (Fig. 2b).

A significant shift of the  $V_{rev}$  of the A23187-induced currents to more positive potentials occurred when extracellular  $\text{Cl}^-$  was replaced by the organic anion glutamate $^-$  in both native *X. laevis* oocytes and mAno1-overexpressing oocytes (Fig. 2c). This finding is consistent with CaCCs, which are known to be much less permeable to organic anions than to  $\text{Cl}^-$  [75].

To quantify the degree of rectification of the A23187-induced currents under the various experimental conditions, we calculated the ratio of outward to inward conductance,  $G_{outward}/G_{inward}$ , also known as the outward rectification index (Fig. 2d). The outward rectification was particularly pronounced when the oocytes were incubated with A23187 in the presence of external  $\text{CaCl}_2$  without flufenamic acid (Fig. 2d). Under all experimental conditions, the degree of outward rectification was more pronounced in the native oocytes than the mAno1-expressing oocytes (left vs. right panel in Fig. 2d). Taken together, these results show that application of the  $\text{Ca}^{2+}$ -ionophore A23187 induced

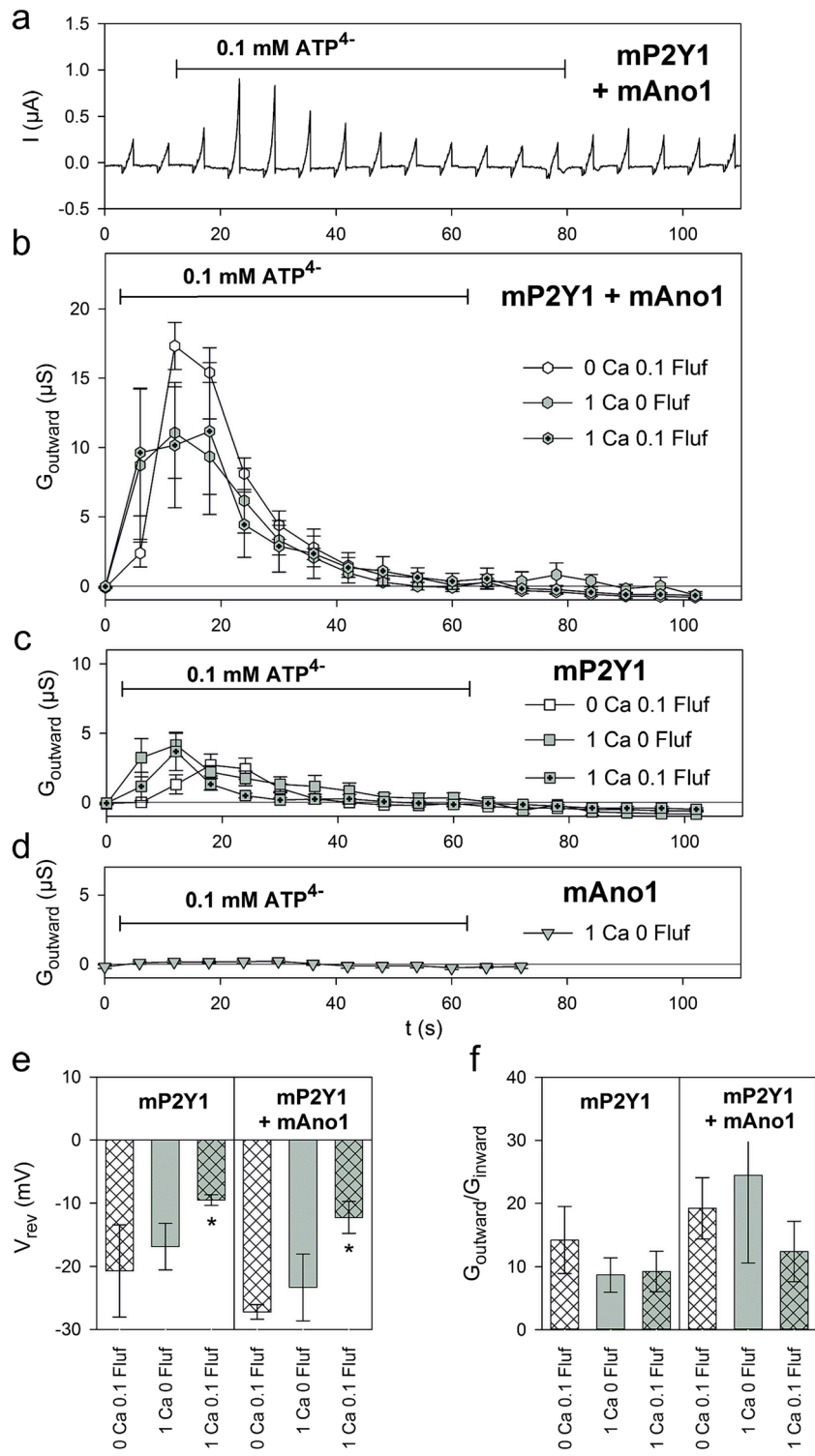
phenotypically similar, but not identical, CaCC currents, which were two- to threefold larger in the mAno1-overexpressing *X. laevis* oocytes than in the native oocytes (Fig. 2a, b).

**Activation of Ano1 by the G protein-coupled purinergic mP2Y1R** Various G protein-coupled receptors, including P2Y receptors, use CaCCs to carry out their physiological functions, and P2Y2R has been shown to activate recombinantly expressed mAno1 [45, 93]. Another P2Y receptor, P2Y1R, is also known to play an important role in controlling  $\text{Cl}^-$  fluxes in airway epithelia and in the release of  $\text{Ca}^{2+}$  from intracellular stores via activating phospholipase C through coupling to  $\text{G}\alpha q$  [64, 88]. We anticipated that P2Y1R might also activate Ano1, and we therefore co-expressed mAno1 with mP2Y1R as a plausible positive control. Indeed, the application of linear voltage-ramp pulses to ATP-stimulated mP2Y1R/mAno1-co-expressing oocytes elicited outwardly directed transient currents, which began to decline over time while ATP was still present (Fig. 3a). These currents reflected a transient increase in membrane conductance (Fig. 3b). A three- to fourfold smaller, but still significant, transient increase in membrane conductance was observed in ATP-stimulated oocytes expressing mP2Y1 alone (Fig. 3c). In contrast, the membrane conductance of oocytes expressing mAno1 alone did not change in response to the application of ATP (Fig. 3d), indicating that P2Y1 was required for the increase in conductance.

Consistent with a current that is activated by  $\text{Ca}^{2+}$  released from intracellular stores, omitting extracellular  $\text{Ca}^{2+}$  did not diminish the ATP-elicited currents in mP2Y1R/mAno1-co-expressing oocytes (Fig. 3b) or in oocytes expressing mP2Y1R alone (Fig. 3c). Both the  $V_{rev}$  of  $-10$  to  $-20$  mV (Fig. 3e), and the strong outward rectifying behavior (indicated by the outward rectification index  $G_{outward}/G_{inward}$ , Fig. 3f) support the view that the ATP-induced increase in conductance was mediated by CaCCs activated via the mP2Y1R-mediated  $\text{Ca}^{2+}$  release. The ATP-induced increase in  $\text{Cl}^-$  conductance observed in oocytes expressing mP2Y1R alone can be best explained as a result of the oocyte's endogenous CaCCs [9, 46, 90], which apparently can also be activated via P2Y1R-mediated  $\text{Ca}^{2+}$  release. Because the transient activation of Ano1 may result from an ATP concentration that is non-saturating at the P2Y1 receptor, we repeated the experiments shown in Fig. 3b using ADP as the agonist (Fig. S1). Application of a P2Y1 receptor-saturating concentration of  $100 \mu\text{M}$  ADP [39] produced a stronger activation of Ano1 than  $100 \mu\text{M}$  ATP. However, similar as ATP, also ADP elicited a transient rather than a sustained activation of the Ano1-dependent  $\text{Cl}^-$  conductance.

**$\text{Ca}^{2+}$ -dependent activation of Ano1 secondary to activation of P2X7R** The high  $\text{Ca}^{2+}$  permeability of P2X7R [22] led us to

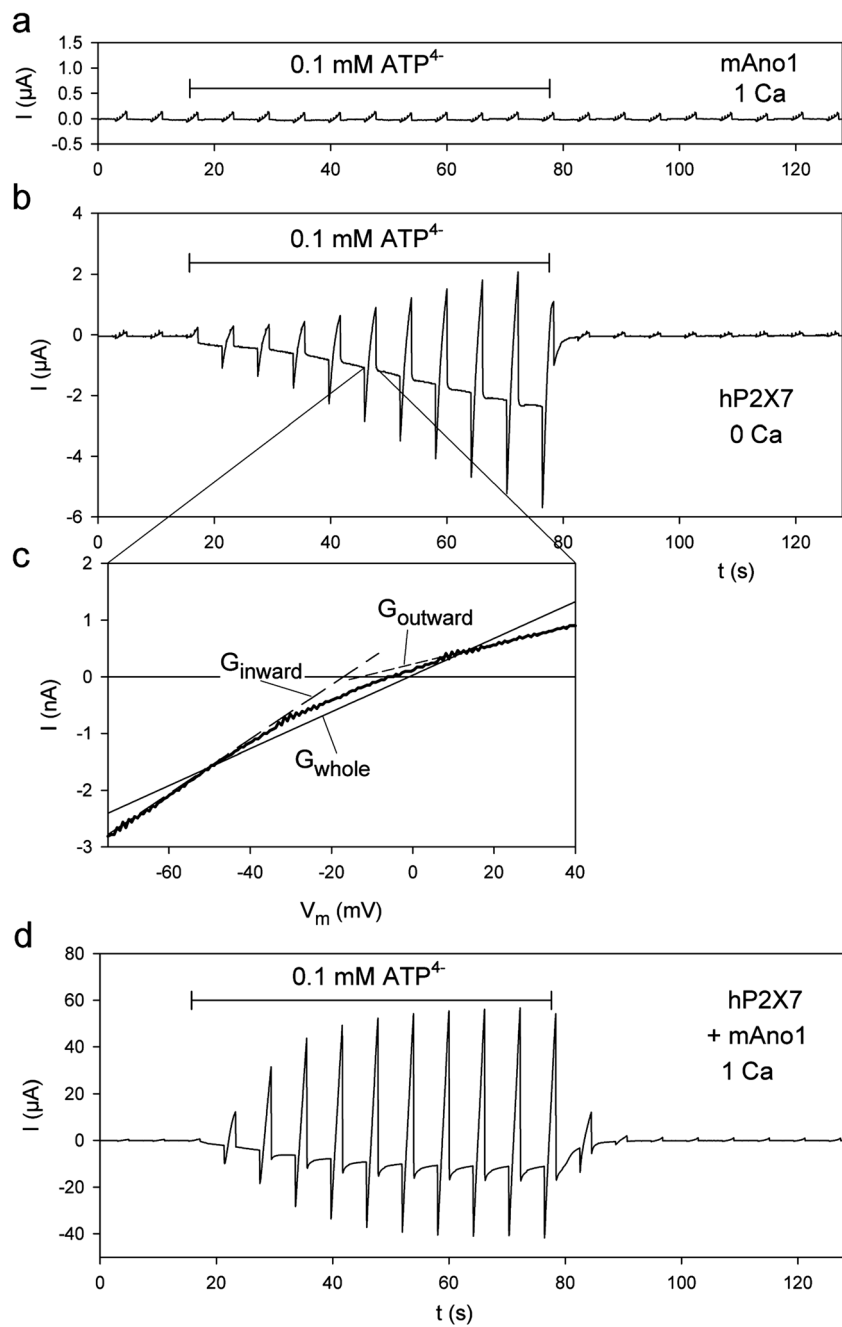
**Fig. 3** Time course of ATP-induced conductance changes in oocytes expressing mAno1 alone, mP2Y1 alone, or both proteins together. **a** The typical current trace shown was recorded from an mP2Y1/mAno1-co-expressing oocyte challenged for 60 s with 0.1 mM ATP<sup>4-</sup> (horizontal bar) in Ca-ORi. **b-d** Following this protocol, the time courses of the ATP-induced changes of the mean outward conductances (mean  $\pm$  SEM from 4–8 oocytes each) were measured in oocytes superfused with the indicated ORi solution and expressing **b** mP2Y1R and mAno1 together, or **c** mP2Y1R alone, or **d** mAno1 alone. The ramp currents recorded before the application of A23187 were subtracted. Notably, the conductances measured 12 and 18 s after ATP application were much larger in the mP2Y1R/mAno1-co-expressing oocytes (**b**) than in oocytes expressing mP2Y1R alone (**c**). **e, f** Bars represent the means  $\pm$  SEM of  $V_{rev}$  and the outward rectification index ( $G_{outward}/G_{inward}$ ) calculated 20 s after the application of ATP. Significant differences between the means are indicated by asterisks. For further explanations, see Fig. 1



examine whether Ano1 channels might be activated secondary to the opening of the P2X7R channel by ATP. To this end, we applied the same voltage-ramp pulses shown in Fig. 1a to hP2X7R-expressing oocytes in the absence and presence of ATP. Typical ramp current traces are shown in Fig. 4. In oocytes expressing mAno1 alone, i.e., without co-expressed

hP2X7R, the voltage-ramp pulses did not evoke ATP-dependent ramp currents (Fig. 4a). In contrast, oocytes expressing hP2X7R alone showed ramp currents whose amplitudes increased continuously during the 1-min application of ATP (Fig. 4b). These recordings were performed in a  $\text{Ca}^{2+}$ -free extracellular solution to prevent the hP2X7R-mediated

**Fig. 4** Time course of ATP-induced currents in oocytes expressing mAno1 alone, hP2X7 alone, or both proteins together. **a**, **b**, **d** The same voltage ramps as shown in Fig. 1a were applied to oocytes expressing mAno1 alone, hP2X7R alone, or both proteins together in the absence or presence of external  $\text{Ca}^{2+}$ , as indicated. ATP was applied for 60 s (horizontal bar). **c** The amplitudes of the selected ramp current from **b** were plotted against the applied membrane potentials to illustrate how the  $G_{\text{inward}}$  and  $G_{\text{outward}}$  conductances were determined from the different slopes of the IV curve. Please note the different scales of the currents in **a**, **b**, **d** and the switch from an outwardly rectifying phenotype in Fig. 1 to inwardly rectifying here



influx of  $\text{Ca}^{2+}$  and the ensuing activation of the endogenous CaCCs. The ramp currents displayed a stronger inward than outward rectification (Fig. 4c), as would be expected if the total current was predominantly carried by cations through the inwardly rectifying ATP-activated P2X7R [40] without significant contamination from the outwardly rectifying CaCC current. At the standard holding potential of  $-40$  mV between ramps, an inward current that increased linearly over time was observed, which is evidently the ATP-activated cation current mediated by hP2X7R in divalent cation-free media [7, 41]. Whether the linearly increasing current is mediated by

hP2X7R itself or a secondarily activated channel distinct from Ano1 has not yet been resolved.

In hP2X7R/mAno1-co-expressing oocytes challenged in a  $\text{Ca}^{2+}$ -containing extracellular solution, the ATP-induced ramp currents were up to tenfold larger and reached a plateau after approximately 40 s of ATP application (Fig. 4d). At the  $-40$  mV holding potential between ramps, mAno1 is likely to pass  $\text{Cl}^-$  out of the cell because the holding potential of  $-40$  mV is negative to the reversal potential of  $\text{Cl}^-$  ( $\sim -10$  mV, Fig. 1d). Accordingly, the linearly increasing inward current must represent the sum of two major currents: the hP2X7R-

mediated  $\text{Na}^+$  and  $\text{Ca}^{2+}$  influx and the CaCC-mediated  $\text{Cl}^-$  efflux. Both currents contribute to the downward deflection of the current trace, as the efflux of negative charges is electrically identical to the influx of the positive charge.

The conductance-based statistical analysis shown in Fig. 5 provides a clearer view of the conductance changes that accompany the application and washout of ATP. The ATP-induced increase in membrane conductance was significantly larger when external  $\text{Ca}^{2+}$  was present, both for oocytes expressing hP2X7R alone (Fig. 5a) and for hP2X7R/mAno1-co-expressing oocytes (Fig. 5b). Consistent with a crucial role of intracellular  $\text{Ca}^{2+}$  levels in the secondary increase in membrane conductance, the ATP-induced conductance increase was largely prevented when the oocytes were pre-injected with the  $\text{Ca}^{2+}$  chelator BAPTA (Fig. 5a, b). The residual conductance increase that persisted in the presence of BAPTA likely represents the true hP2X7R-mediated  $\text{Na}^+$  and  $\text{Ca}^{2+}$  cation conductance.

The co-expression of mAno1 not only doubled the magnitude of the conductance increase but also accelerated the rate of this increase (compare Fig. 5a and b). To provide a quantitative estimate of this acceleration, we calculated the ratio of the conductances observed 60 and 6 s after the addition of ATP ( $G_{60s}/G_{6s}$ ). A high  $G_{60s}/G_{6s}$  ratio, which is indicative of a slow rate of conductance increase, was observed in oocytes expressing hP2X7R alone and challenged with ATP in the presence of external  $\text{Ca}^{2+}$  (Fig. 5c). In contrast, the low  $G_{60s}/G_{6s}$  ratio recorded in hP2X7R/mAno1-co-expressing oocytes indicated a faster conductance increase, suggesting that heterologously expressed mAno1 is activated more rapidly than oocyte-endogenous xAno1. Overall, the secondary activation of the co-expressed Ano1 appears to closely follow the activation of hP2X7R.

Additionally, the deactivation time course of the hP2X7R-dependent total ATP-induced current following ATP washout was dependent on mAno1 co-expression and the presence of extracellular  $\text{Ca}^{2+}$ . The larger conductance elicited by the ATP stimulation of hP2X7R/mAno1-co-expressing oocytes with  $\text{Ca}^{2+}$  in the bath was associated with slower deactivation of the conductance (compare Fig. 5a and b). A plausible explanation for this result is that the conductance deactivation is dominated by the time course of CaCC deactivation, which in turn reflects the decline in the submembranous  $\text{Ca}^{2+}$  level due to  $\text{Ca}^{2+}$  re-sequestration and extrusion when the  $\text{Ca}^{2+}$  influx through hP2X7R ceases. In excised patches, the closing of hP2X7R occurs at a much faster rate [68] than suggested by the decay of the total conductance in whole-oocyte current recordings (Fig. 5a, b).

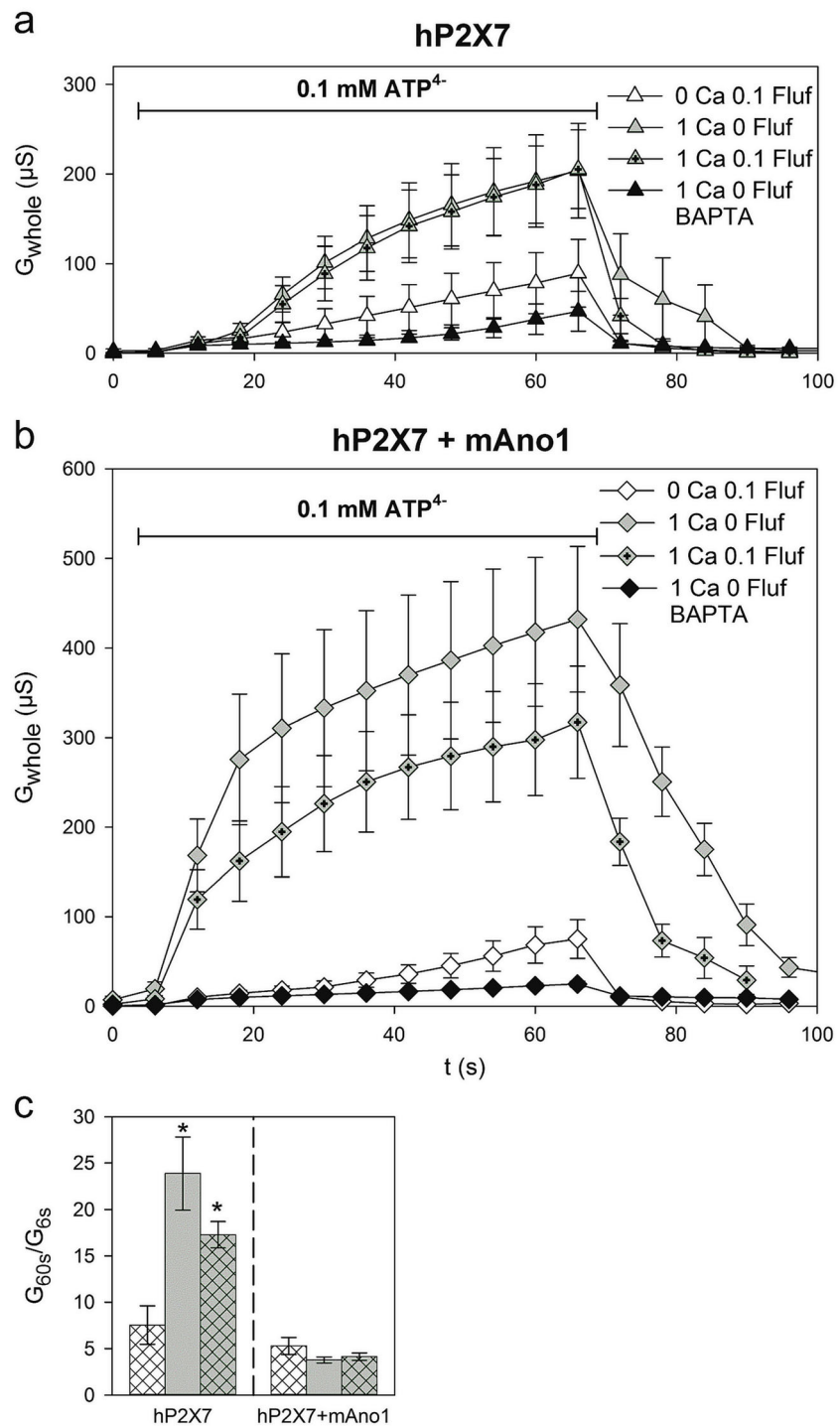
**Evidence that the hP2X7-mediated increase in cytosolic  $\text{Ca}^{2+}$  increases  $\text{Cl}^-$  conductance** To verify that the increase in  $[\text{Ca}^{2+}]_i$  resulted in an increase in  $\text{Cl}^-$  conductance, we comparatively determined  $V_{\text{rev}}$  in  $\text{Cl}^-$ - and glutamate $^-$ -based

media. Replacing external  $\text{Cl}^-$  with the much-less-permeant glutamate $^-$  should induce a shift of  $V_{\text{rev}}$  to a more positive potential if  $\text{Cl}^-$  conductance contributes substantially to the total conductance. Indeed, the substitution of glutamate $^-$  for  $\text{Cl}^-$  produced a positive  $V_{\text{rev}}$  shift when hP2X7R-expressing oocytes (left panel of Fig. 6a) or hP2X7R/mAno1-co-expressing oocytes (left panel of Fig. 6c) were stimulated with ATP in the presence of external  $\text{Ca}^{2+}$ . No such positive  $V_{\text{rev}}$  shift was observed in the  $\text{Ca}^{2+}$ -free glutamate $^-$ -based medium (left panels of Fig. 6a, c), highlighting the importance of the  $\text{Ca}^{2+}$  influx for the activation of the  $\text{Cl}^-$  conductance. The glutamate $^-$ -induced positive shift of  $V_{\text{rev}}$  was also suppressed when oocytes expressing hP2X7R, either alone or together with mAno1, were pre-injected with BAPTA (right panels of Fig. 6a, c). The more-pronounced positive  $V_{\text{rev}}$  shift observed in the mAno1-expressing oocytes (compare Fig. 6a and c) is consistent with the expected larger contribution of CaCC conductance to whole-cell conductance upon the overexpression of mAno1.

To provide evidence of the simultaneous activation of hP2X7R and endogenous CaCCs or overexpressed mAno1, we took advantage of the fact that the current–voltage relationships of P2X7R and the Ano1 channel show rectifying characteristics in opposite directions (inward and outward, respectively) (Figs. 2d and 4d). Consistent with the  $[\text{Ca}^{2+}]_i$ -dependent activation of an overlapping outwardly rectifying conductance reflecting the activation of endogenous CaCCs, the inward rectification attributable to the ATP-activated hP2X7R was reduced in  $\text{Ca}^{2+}$ -containing ORi compared to  $\text{Ca}^{2+}$ -free ORi (Fig. 6b, left panel). In hP2X7R/mAno1-co-expressing oocytes, the rectification was even converted from inward to outward in  $\text{Ca}^{2+}$ -containing ORi (Fig. 6d, left panel), consistent with a large increase in mAno1-mediated  $\text{Cl}^-$  conductance under these conditions. In accord with the increase of intracellular  $\text{Ca}^{2+}$  required for the increase in  $\text{Cl}^-$  conductance, the extracellular  $\text{Ca}^{2+}$ -dependent changes in the rectifying characteristics were prevented in BAPTA-pre-injected oocytes (right panels of Fig. 6b, d).

***hAno6 is not activated by the  $\text{Ca}^{2+}_i$  increase mediated by A23187 or hP2X7*** The above experiments provide clear evidence that Ano1-mediated  $\text{Cl}^-$  conductance can be activated by an increase in  $[\text{Ca}^{2+}]_i$  resulting from  $\text{Ca}^{2+}$  influx through the ATP-activated hP2X7 receptor. Controversial functions have been assigned to Ano6, including a role as a  $\text{Ca}^{2+}_i$ -dependent anion channel [32, 42, 78]. We therefore tested whether increasing  $[\text{Ca}^{2+}]_i$  through application of the  $\text{Ca}^{2+}$  ionophore A23187 or sustained ATP stimulation of hP2X7R elicits increased conductance in *Xenopus* oocytes expressing hAno6 alone or together with hP2X7R (Fig. 7). However, rather than the expected increase in outward conductance, we observed that A23187 significantly decreased the outward conductance in hAno6-expressing *Xenopus* oocytes (Fig. 7a).

**Fig. 5** Time course of conductance changes following ATP activation of hP2X7R, either alone or co-expressed with mAno1. The data represent the means $\pm$ SEM from 4–10 oocytes per condition. **a, b** Time course of the total ramp conductance, G (means $\pm$ SEM from 4–8 oocytes per data point), following the application of 0.1 mM ATP<sup>4-</sup> to oocytes expressing hP2X7R, either alone or together with mAno1, and superfused with the indicated ORI solution. Black-filled symbols represent recordings from oocytes that were pre-injected with BAPTA. The conductances were significantly larger in Ca<sup>2+</sup>-containing ORI than in Ca<sup>2+</sup>-free ORI or in oocytes pre-injected with BAPTA. **c** The total ramp conductance increased more rapidly in mAno1/hP2X7-co-expressing oocytes than in oocytes expressing hP2X7 alone, as inferred from the low G<sub>60s</sub>/G<sub>6s</sub> conductance ratios calculated from the absolute conductance determined 60 and 6 s after the addition of ATP. For further explanations, see Fig. 1



In addition, the hP2X7R-elicited conductance increase was lower in the hAno6/hP2X7R-expressing oocytes than in the *Xenopus* oocytes expressing hP2X7R alone (Fig. 7b). The outward rectification did not change upon co-expression of hAno6: following a 40-s treatment with ATP in Ca<sup>2+</sup>-containing bathing solution, the outward rectification index (G<sub>outward</sub>/G<sub>inward</sub>) was 0.99 $\pm$ 0.01 or 0.97 $\pm$ 0.02 for *Xenopus* oocytes

expressing hP2X7 or hP2X7/hAno6, respectively. These values are not significantly different from the rectification indices calculated from recordings of hP2X7R-expressing *Xenopus* oocytes activated with ATP in a Ca<sup>2+</sup>-containing bath (see Fig. 6b, d). We conclude that the hP2X7R-mediated Ca<sup>2+</sup> influx was not capable of activating an outwardly rectifying conductance in hP2X7R/hAno6-expressing

*Xenopus* oocytes. In contrast, a  $\text{Ca}^{2+}$ -dependent outwardly rectifying conductance could be elicited in native lymphocytes [42].

Finally, as an additional control, we repeated the most essential experiments in Axolotl oocytes because Axolotl oocytes in contrast to *Xenopus* oocytes lack endogenous CaCCs [75]. We found that an A23187-induced increase in the outward conductance in Axolotl oocytes required the expression of mAno1 (Fig. 7c), consistent with the absence of endogenous CaCCs in Axolotl oocytes. This finding indirectly supports the view that A23187-induced conductance increase seen in native *Xenopus* oocytes is mediated by endogenous CaCC(s). Similar as in *Xenopus* oocytes, application of ATP produced a larger increase in the total conductance in hP2X7R/mAno1-expressing Axolotl oocytes than in Axolotl oocytes expressing the hP2X7R alone (Fig. 7d). Whether the hP2X7R-dependent conductance recorded in the absence of co-expressed mAno1 represents exclusively the hP2X7R-mediated  $\text{Na}^+$  and  $\text{Ca}^{2+}$  influx or includes any other secondarily activated channel conductance cannot be inferred from our data.

No increase in the  $\text{Cl}^-$  conductance in response to A23187 or ATP was seen in Axolotl oocytes expressing hAno6 alone (Fig. 7c, d). When hAno6 was co-expressed with the hP2X7, the application of ATP resulted even in a smaller conductance

increase than seen in Axolotl oocytes expressing the P2X7 alone (Fig. 7d). Taken together, the mAno1- and hAno6-mediated conductance changes in Axolotl oocytes are fully compatible with those in *Xenopus* oocytes.

*Ano6 assembles as a non-covalent homodimer in *X. laevis* oocytes, similar to Ano1* Because the electrophysiological experiments provided no evidence of hAno6 and mAno6 functioning as CaCCs, we tested their expression as plasma membrane-bound proteins and determined their oligomeric states in *X. laevis* oocytes. To this end, we purified hexahistidine-tagged versions of mAno1, hAno6, and mAno6 following metabolic and covalent cell-surface labeling with [ $^{35}\text{S}$ ]-methionine and the Cy5-NHS or IR800-NHS dye, respectively. We knew from previous experiments that N- or C-terminal hexahistidine-tagging does not adversely affect the CaCC function of mAno1 [24]. We used digitonin as a mild detergent to perform membrane protein solubilization [72, 73]; in contrast to dodecylmaltoside, digitonin stably preserves the homodimeric architecture of mAno1 [24].

Resolution of the purified proteins via SDS-PAGE followed by fluorescence scanning showed that hAno6 and mAno6 were expressed at the plasma membrane of *X. laevis* oocytes (Fig. 8a, lanes 2–3), but at a markedly lower abundance than mAno1 (Fig. 8a, lane 1, the fluorescence signal of mAno1

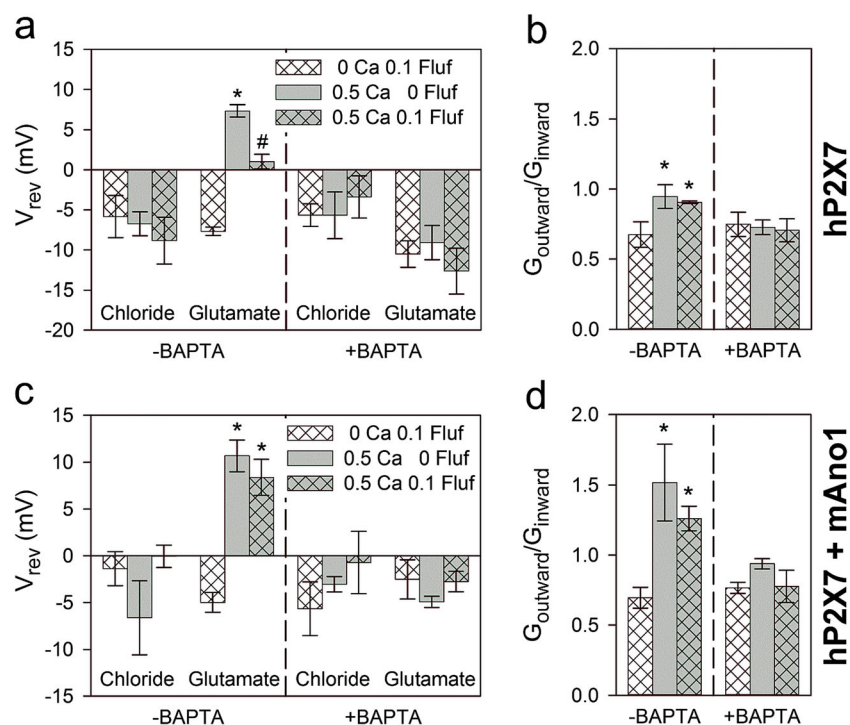


**Fig. 6** Characterization of ionic currents elicited by ATP in oocytes expressing P2X7R alone and together with mAno1.  $V_{\text{rev}}$  and the outward rectification index,  $G_{\text{outward}}/G_{\text{inward}}$ , were determined as illustrated in Fig. 1d in oocytes expressing P2X7R, either alone (a, b) or together with mAno1 (c, d). The oocytes were stimulated with ATP in both  $\text{Ca}^{2+}$ -free and  $\text{Ca}^{2+}$ -containing ORI, as indicated. Where indicated

by “+BAPTA,” the oocytes were pre-injected with the  $\text{Ca}^{2+}$  chelator BAPTA 1–2 h before the currents were recorded. “Chloride” and “Glutamate” specify the principle anion in the ORI solution in which the recordings were taken. Bars represent the means  $\pm$  SEM from 4–10 oocytes per group. Significantly different means are indicated by different symbols. For further explanations, see Fig. 1

shown was fivefold attenuated compared to Ano6 by ImageQuant settings). Of note, the SDS-denatured and chemically reduced *N*-glycosylated forms of hAno6 (913 residues) and mAno6 (911 residues) both migrated in the SDS-urea-PAGE gel with an anomalously low mass of only ~83 kDa compared to the sequence-predicted protein cores of 107 and 106 kDa, respectively. Migration at a lower-than-predicted mass in the SDS-PAGE gel is commonly found with multispan membrane proteins [28, 66]. Also, mAno1 exhibited this negative mass shift by migrating at only ~105 kDa (Fig. 8a, lane 1) instead of >126 kDa expected for a 111 kDa protein (956 residues) having five *N*-glycans [24]. It has been suggested that the retention of SDS-resistant helix-helix interactions may result in a more compact structure that accounts for the higher SDS-PAGE mobility of multispan membrane proteins [63]. Indeed, using BN-PAGE and the partially disassembled pentameric 5HT<sub>3</sub>R as a mass marker yielded significantly larger masses for each of the anoctamin protomers (see text below to Fig. 8b).

Next, we analyzed non-denatured hAno6 and mAno6 via BN-PAGE to determine their quaternary structure. We have

previously shown that BN-PAGE is capable of faithfully displaying the quaternary structures of integral membrane proteins [17, 28, 31, 55, 57] as well as those of soluble proteins, such as the multimeric scaffolding protein gephyrin [70]. Non-denatured hAno6 and mAno6 (Fig. 8b, lanes 3 and 5) each migrated as a distinct band in the BN-PAGE gels. Using the 256-kDa band of the homotetrameric 5HT<sub>3</sub>R intermediate and the 320-kDa band of the non-disassembled homopentameric 5HT<sub>3</sub>R as mass markers (Fig. 8b, oval symbols), the apparent masses of the hAno6 and mAno6 were estimated to be ~290 kDa. In comparison, non-denatured mAno1 migrated at ~320 kDa (Fig. 8b, lane 1) as previously reported [24]. Incubation of hAno6 and mAno6 with 0.1 % SDS resulted in complete disassembly of the ~290 kDa band and the appearance of a faster-migrating band at ~150 kDa (Fig. 8b, lanes 4 and 6), as estimated by referring to the dimeric and trimeric forms of the disassembled 5HT<sub>3</sub>R (Fig. 8b, oval symbols). The apparent protomer masses of ~150 kDa, including *N*-linked complex carbohydrates, observed in the BN-PAGE gel can be well reconciled with the sequence-predicted 107 and 106 kDa for the carbohydrate-

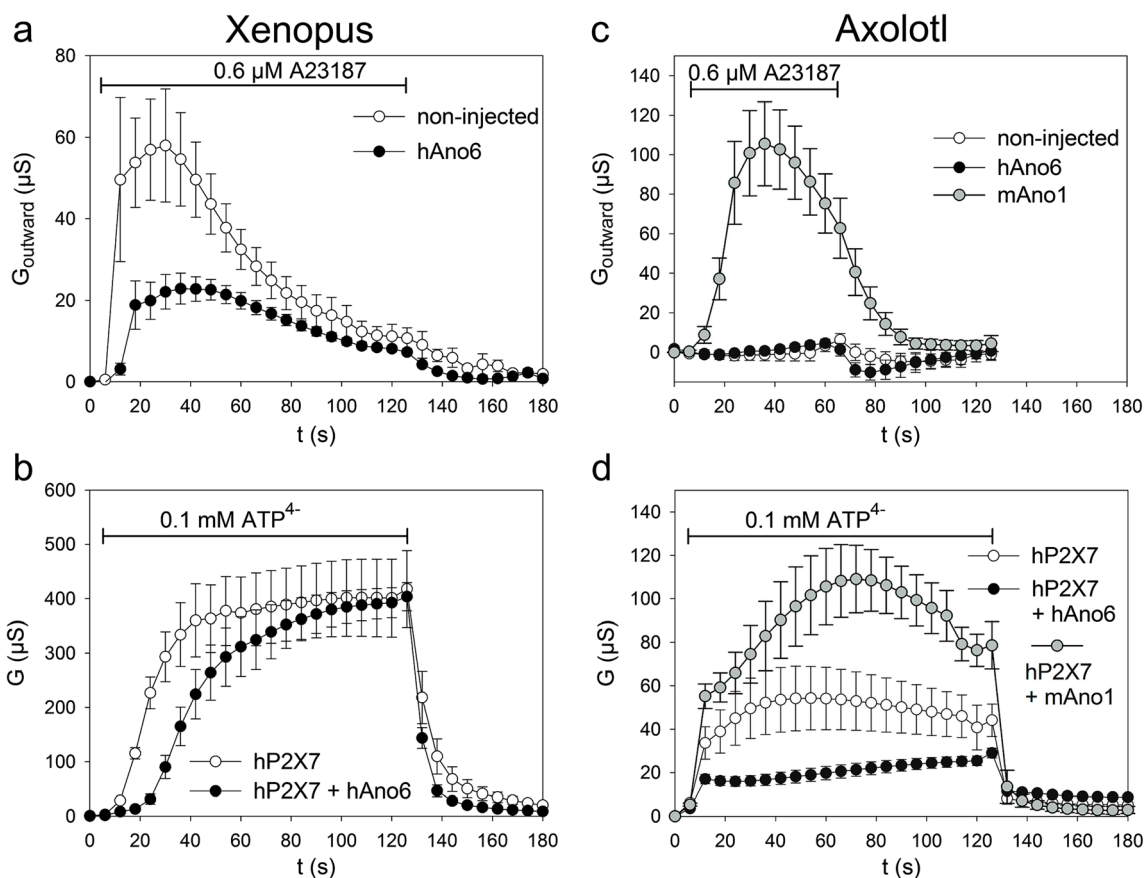


**Fig. 7** Conductance changes elicited by A23187 or ATP in oocytes expressing mAno1 or hAno6 alone or together with hP2X7. **a:** Xenopus oocytes; **c, d:** Axolotl oocytes. *Upper panels* time course of the outward ramp conductance,  $G_{\text{outward}}$ , induced by the application of A23187 in native or mAno1- or Ano6-expressing oocytes, as indicated.

*Lower panels* time course of the whole ramp conductance induced by the application of ATP to oocytes expressing hP2X7R, either alone or together with mAno1 or hAno6, as indicated. All measurements were performed in Ca-ORI. The data points represent the means±SEM from 6-15 oocytes per data point

free protein cores of hAno6 and mAno6, respectively. Because no faster-migrating band was observed, it is safe to conclude that the ~150-kDa bands represent the protomeric forms of hAno6 and mAno6. Accordingly, the non-denatured ~290-kDa band must be the homodimer of Ano6, which indicates that Ano6 shares a homodimeric architecture with Ano1.

*Ano1 and Ano6 assemble as non-covalent homodimers in Axolotl oocytes* Next, we examined the oligomeric state of Ano1 and Ano6 in Axolotl oocytes known to be devoid of endogenous CaCCs. The plasma membrane-bound mAno1 could be well-detected in the BN-PAGE gel as a 340 kDa protein that disassembled into a 170 kDa protomer when

incubated with 0.1 % SDS (Fig. 9, lanes 3 and 4). This indicates that mAno1 existed also in Axolotl oocytes as a homodimer, but migrated at a somewhat higher mass than the mAno1 purified from *X. laevis* oocytes (~340 vs. 320 kDa). This mass difference seems to reflect species-specific differences in the size of the complex-type carbohydrates (see Fig. 10, compare lanes 1–3 with 4–6).

In contrast, the plasma membrane-bound forms of mAno6 and hAno6 were barely, if at all, detectable in the BN-PAGE gel even at maximum enhancement of the fluorescence signal (Fig. 9, lanes 5–8). However, the homodimeric and protomeric states of Ano6 from Axolotl oocytes were unequivocally visible in the [<sup>35</sup>S]-methionine-labeled total form. Masses of 280 and 260 kDa for the homodimeric forms of

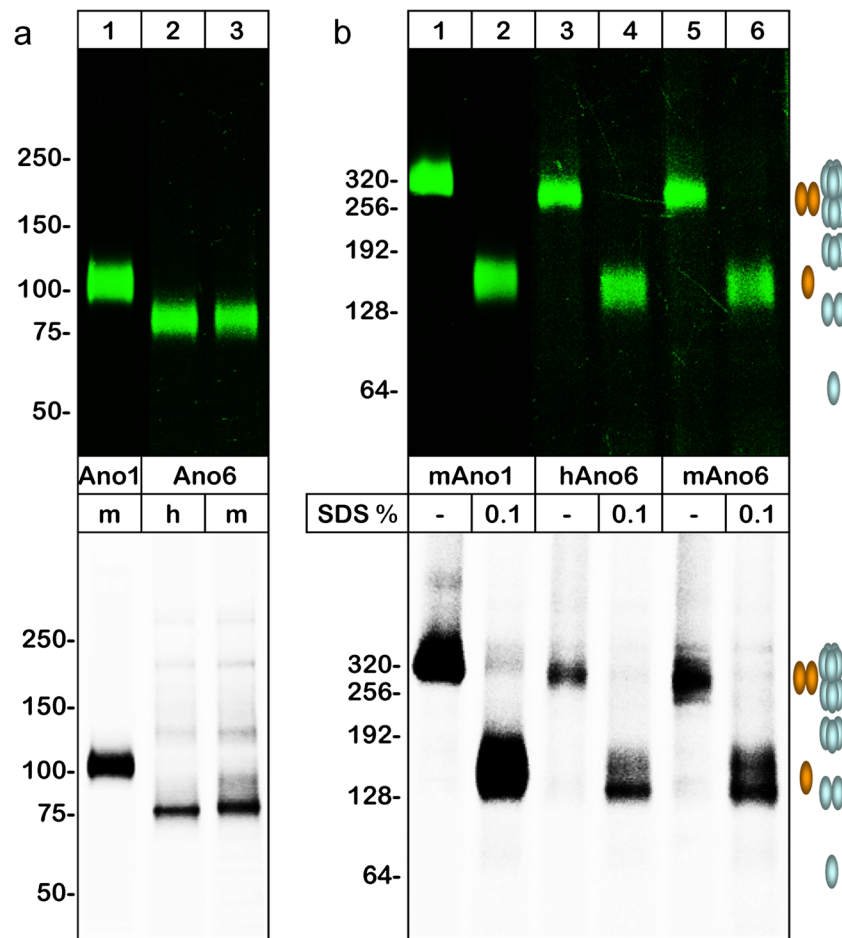


**Fig. 8** Total expression, cell-surface expression, and quaternary structure of Ano6. mAno1-His, hAno6-His, and mAno6-His (*m* mouse; *h* human) were purified via non-denaturing Ni-NTA chromatography from digitonin extracts of *X. laevis* oocytes. **a** Protomeric state in *Xenopus* oocytes. The proteins were denatured using 2 % SDS and 20 mM DTT, resolved through SDS-urea-PAGE, and visualized in the Cy5-labeled plasma membrane-bound form or [<sup>35</sup>S]-methionine-labeled total form via Typhoon fluorescence scanning (upper panels) or phosphorimaging (lower panels), respectively. Of note, Ano1 and Ano6 migrate with a lower apparent mass than predicted from their amino acid sequences, as is the case with the majority of large multispan membrane proteins [66]. **b**

Oligomeric state in *Xenopus* oocytes. The protein migration of the same samples as in **a** is shown both under native conditions and following partial denaturation after a 1-h incubation with 0.1 % SDS at 37 °C, as indicated. The blue ovals schematically illustrate the oligomeric states of the partially denatured 5HT<sub>3</sub>R, which resolves in the BN-PAGE gels as a ladder of partially disassembled proteins consisting of one to five 64 kDa protomers (protomers to pentamers), thus serving as a versatile membrane-bound mass marker. The orange ovals schematically illustrate the native homodimeric and denatured protomeric states of Ano6 and, for comparison, Ano1

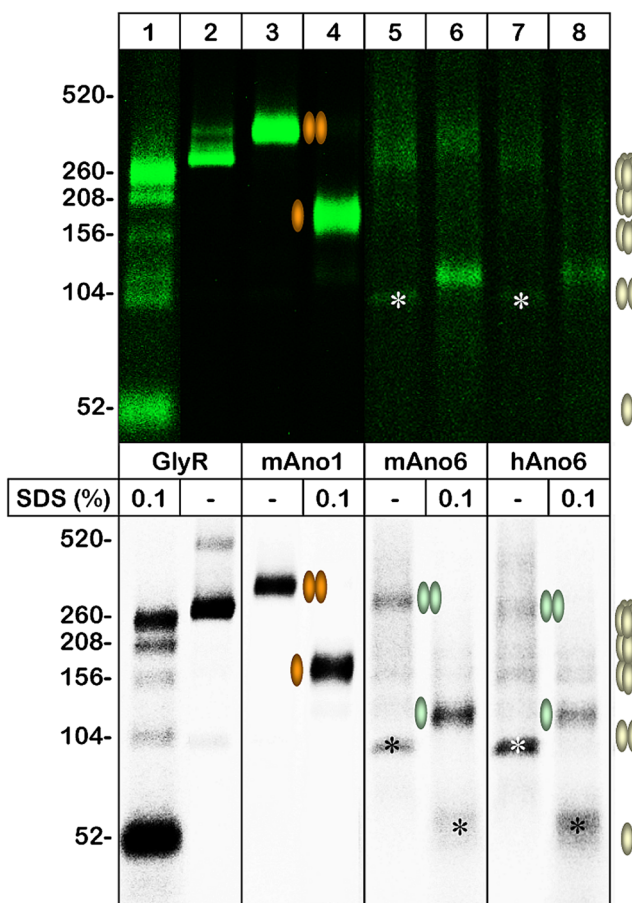


**Fig. 9** Quaternary structure of mAno1 and Ano6 expressed in Axolotl oocytes. The indicated proteins were purified and analyzed by BN-PAGE as described in the legend to Fig. 8 except that IR800-NHS ester was used for cell-surface labeling instead of Cy5 NHS ester. The yellow ovals schematically illustrate the oligomeric states of the partially denatured GlyR, which resolves in the BN-PAGE gels as a ladder of partially disassembled proteins consisting of one to five 52 kDa protomers. The orange and green ovals schematically illustrate the native homodimeric and denatured protomeric states of mAno1 (orange) and Ano6 (green). Asterisk denotes background band

mAno6 and hAno6, respectively, and 121 kDa for the protomeric forms were assessed by comparison with the appropriate oligomeric states of the partially disassembled GlyR.

*mAno6, in contrast to mAno1, is mostly retained in the endoplasmic reticulum* mAno1 existed in the plasma membrane, and the [ $^{35}$ S]-methionine-labeled total form entirely in the EndoH resistant and hence mature complex-glycosylated form (Fig. 10, lanes 1–6, upper and lower panels). This indicates that mAno1 was efficiently trafficked from the endoplasmic reticulum to the Golgi and later compartments in Axolotl and *X. laevis* oocytes. Also, mAno6 appeared as a complex-glycosylated protein in the plasma membrane of *X. laevis* oocytes (Fig. 10, lanes 10–12, upper panel). In the plasma membrane of Axolotl oocytes, mAno6 was below detectability (Fig. 10, lanes 7–9, lower panel). The low or

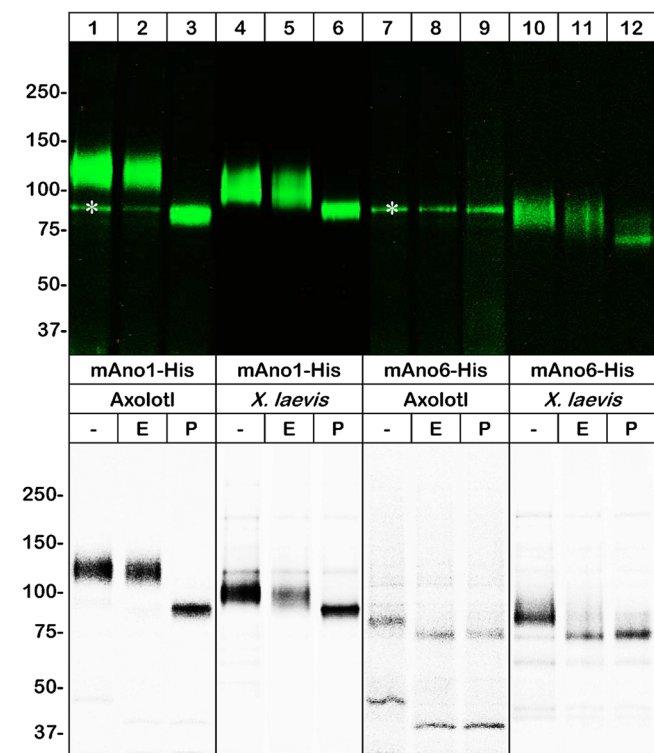


**Fig. 10** *N*-glycosylation state of Ano1 and Ano6 in oocytes of Axolotl and *Xenopus*. Aliquots of the same protein samples as used in Fig. 9 and similar samples as used in Fig. 8, from Axolotl oocytes and *Xenopus* oocytes, respectively, were deglycosylated with EndoH (E) or PNGase F (P), as indicated. mAno1 was largely EndoH-resistant both in the plasma membrane-bound form and the [ $^{35}$ S]-methionine-labeled total form. In contrast, the [ $^{35}$ S]-methionine-labeled total form of Ano6 was largely EndoH sensitive. In Axolotl oocytes, mAno6 could be only detected in the [ $^{35}$ S]-methionine-labeled form, but not in the plasma membrane-bound form. Asterisk denotes background band

lacking plasma membrane expression of mAno6 coincided with the retention of most of mAno6 in the endoplasmic reticulum, as evidenced by the distinct EndoH sensitivity of the [ $^{35}$ S]-methionine-labeled form of mAno6 (Fig. 10, lanes 7–12, lower panel). These data are fully consistent with the previously observed retention of Ano6 in the endoplasmic reticulum of various mammalian cell lines including HEK293, CHO, and COS-7 cells [21].

*Ano1 and Ano6 do not stably interact with co-expressed hP2X7R* To screen for a physically stable interaction between P2X7R and Ano1 or Ano6, we co-expressed His-hP2X7R as a bait protein together with hAno1-His or hAno6-His as the prey. Purifying the His-tagged proteins from digitonin extracts of cells via metal affinity chromatography allowed us to verify the presence of hP2X7R and hAno1 (Fig. 11a, lanes 1–2, 4, 6) or hP2X7R and hAno6 (Fig. 11b, lanes 1–2, 4, 6). For pull-down from aliquots of the same non-denatured digitonin extracts, we used a monoclonal antibody against hP2X7R that immunoprecipitated hP2X7R when expressed alone (Fig. 11a, lane 7) but did not immunoprecipitate either hAno1 (Fig. 11a,

lane 8) or hAno6 (data not shown) when expressed alone. The monoclonal antibody also reliably immunoprecipitated hP2X7R from extracts of cells co-expressing hAno1/hP2X7R (Fig. 11a, lanes 3 and 5) or hAno6/P2X7R (Fig. 11b, lanes 3 and 5). However, we did not obtain any evidence of co-precipitation of hAno1 or hAno6, arguing against a stable interaction with hP2X7R. Additionally, increasing the relative amount of injected hAno1-His cRNA over His-hP2X7 cRNA (Fig. 11a, lanes 5–6) or of His-hP2X7 cRNA over hAno6-His cRNA (Fig. 11b, lanes 5–6) did not affect this overall result.

**Interaction of P2X7R and Ano1 in pancreatic cells** To demonstrate that P2X7R and Ano1 interact not only in a recombinant system, but also in native cells, we performed whole-cell patch clamp experiments in the pancreatic adenocarcinoma cell line, AsPC-1. The rationale was that P2X7R [59] and Ano1 [59, 74] are both expressed in the pancreas and Ano1 is expressed and functional in AsPC-1 cells [71]. In K<sup>+</sup>-free and low Cl<sup>-</sup> intracellular solution and extracellular solution lacking K<sup>+</sup> and Na<sup>+</sup> to suppress Na<sup>+</sup> and K<sup>+</sup> currents, application of the P2X7R agonist BzATP (Fig. 12a–c) or the Ca ionophore A23187 (Fig. 12d–f) induced similar outwardly rectifying currents (for statistics, see Fig. 12l, m). The increase of these currents during the several s-lasting application of

BzATP or A23187 was associated with a shift of the reversal potential to more negative potentials concordant with the applied transmembrane Cl<sup>-</sup> gradient (Fig. 12n, see also the “Materials and methods” section). Shortly after application of BzATP, a current without outward rectification was measured, which may be in part mediated by the influx of Tris cations through the P2X7R (Fig. 12a; [69]) but is probably to a greater extent mediated by Ano1 (see below). When the Ca<sup>2+</sup> level of the internal solution was strongly buffered by EGTA and BAPTA, BzATP activated no measurable current in the Tris-based external solution (Fig. 12g, h) or only the inwardly rectifying P2X7R-mediated current in the Na<sup>+</sup>-based extracellular solution (Fig. 12i). These observations indicate that the development of the outwardly rectifying currents shown in Fig. 12b, c, e, f (and partially in Fig. 12a, d) were mediated by rises in the intracellular Ca<sup>2+</sup> levels (Fig. 12g–i).

## Discussion

**P2Y1R and P2X7R couple functionally with Ano1 but not Ano6** In this work, we demonstrate that the activation of the purinergic receptors mP2Y1R and hP2X7R by ATP in *X. laevis* oocytes can secondarily activate endogenous CaCCs or recombinantly expressed mAno1 (but not recombinant

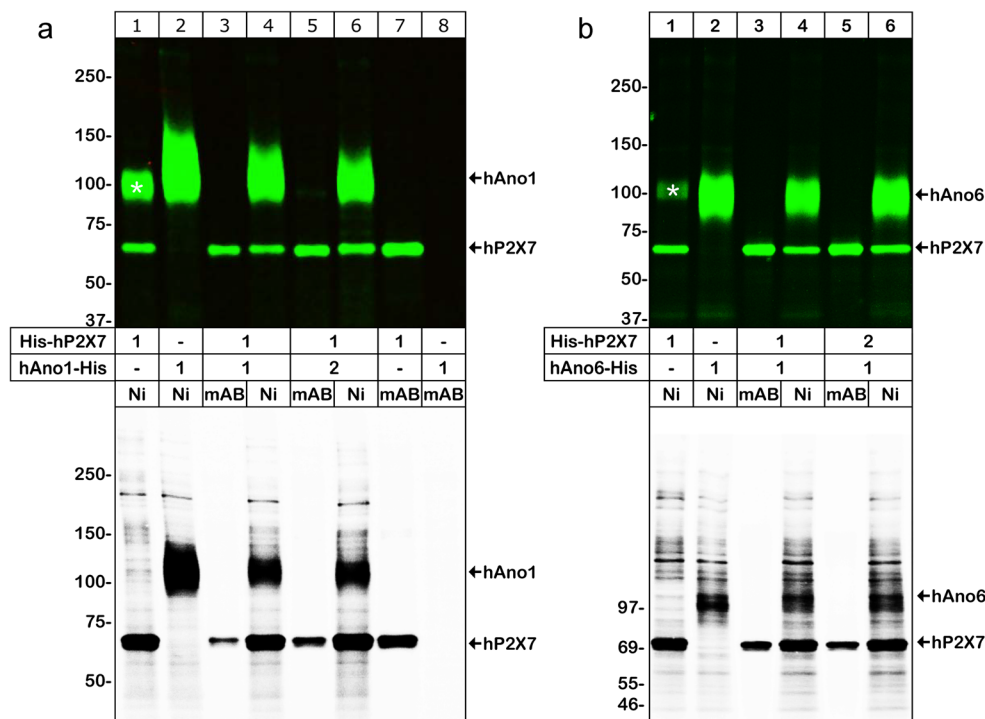


**Fig. 11** Neither hAno1 nor hAno6 co-purifies with hP2X7R. Oocytes expressing His-hP2X7 and hAno1-His or hAno6-His, either alone or in combination, as indicated, were labeled as in Fig. 8, except that IR800-NHS ester was used instead of Cy5-NHS ester. The numbers (1 or 2) in the figure legends indicated the relative amount of the corresponding cRNA injected. Proteins were isolated in parallel from aliquots of the

same non-denatured digitonin extracts via Ni-NTA chromatography (Ni) or immunoprecipitation with a monoclonal antibody against hP2X7R (mAB), as indicated. **a** hP2X7R/hAno1; **b** hP2X7R/hAno6. *Upper panels* plasma membrane-bound proteins; *lower panels* total [<sup>35</sup>S]-methionine-labeled protein. The asterisks indicate a nonspecific background band of unclear origin

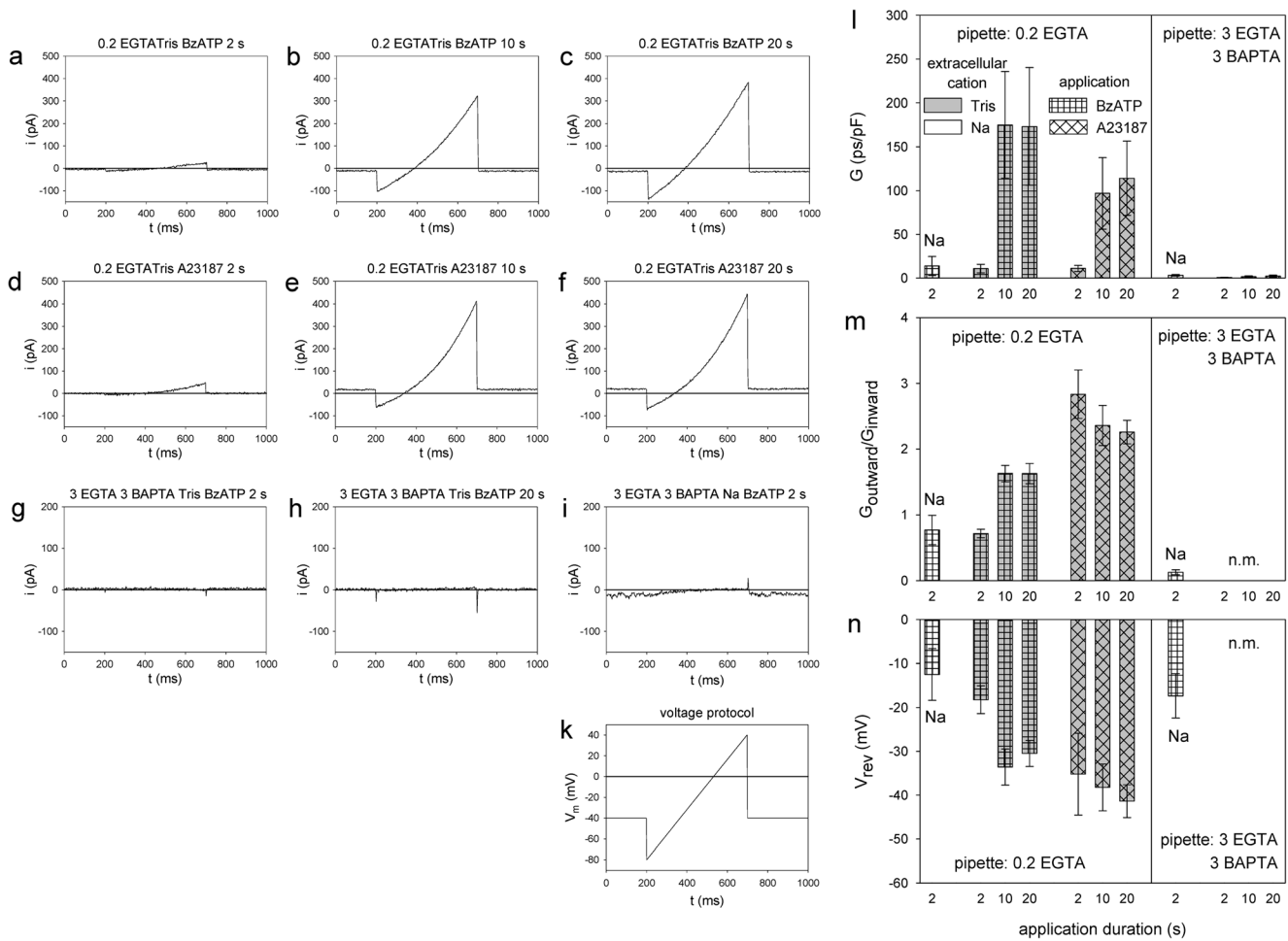


**Fig. 12** Activation of  $\text{Ca}^{2+}$ -dependent currents in human pancreatic cells via the P2X7R. **a–i** Examples of ramp currents evoked by application of 0.1 mM BzATP<sup>4-</sup> (**a–c**, **g–i**) or 1  $\mu\text{M}$  A23187 (**d–f**) in extracellular solution containing  $\text{Tris}^+$  (**a–h**) or  $\text{Na}^+$  (**i**). The intracellular solution was  $\text{Ca}^{2+}$  buffered with 0.2 mM EGTA (**a–f**) or 3 mM EGTA and 3 mM BAPTA (**g–i**). The variant components of the internal and

external solutions are indicated on the top of the figures. Na denotes measurements in  $\text{Na}^+$ -containing extracellular solution. **k** Ramp voltage protocol. **l–m** Statistics of the BzATP- or A23187-induced ramp currents with **l** slope conductance at  $V_{\text{rev}}$ , **m** outward rectification index, and **n** reversal potential. *n.m.* not measured because of tiny currents. Means  $\pm$  SEM from 5–9 cells

mAno6) by causing an increase in intracellular  $\text{Ca}^{2+}$ : (i) application of extracellular ATP increased  $\text{Cl}^-$  conductance in oocytes expressing mP2Y1R or hP2X7R either alone or together with mAno1, but not in native oocytes or oocytes expressing mAno1 alone; and (ii) the increase in  $\text{Cl}^-$  conductance was attenuated when the intracellular  $\text{Ca}^{2+}$  increase was dampened by the prior injection of BAPTA. It is now clear that the oocyte-endogenous CaCC currents are predominantly, if not solely, mediated by *Xenopus* Ano1 (xAno1). xAno1 was obtained through expression cloning from *X. laevis* oocytes using oocytes of the Axolotl salamander *Ambystoma mexicanum* that are devoid of endogenous CaCC activity [75]. The Ano1 sequences of *X. laevis* and mice share 77 % sequence identity (93 % similarity), as determined via Clustal Omega analysis. The coupling of P2X7R to Ano1 appears to be merely functional, as in a non-denaturing co-purification

assay, we obtained no biochemical evidence of a stable physical association of the hP2X7R receptor with mAno1.

G protein-coupled receptors (GPCRs) can utilize the oocyte-endogenous second-messenger system to activate intracellular  $\text{Ca}^{2+}$  release and, subsequently, endogenous CaCCs, which has been well-documented for various GPCRs, including serotonin receptors and P2Y2R [45, 83, 93]. Consistent with GPCR/IP3-mediated elevation of  $\text{Ca}^{2+}$  levels exclusively through  $\text{Ca}^{2+}$  release from intracellular stores, the mP2Y1R-mediated increase in CaCC conductance observed here was virtually of the same magnitude, independent of whether  $\text{Ca}^{2+}$  was present in the bath. In contrast, the hP2X7R-elicited increase in  $\text{Cl}^-$  conductance was approximately tenfold larger when extracellular  $\text{Ca}^{2+}$  was present, indicating that  $\text{Ca}^{2+}$  influx through the opened hP2X7R is a much more powerful activator of endogenous or

overexpressed Ano1 than  $\text{Ca}^{2+}$  release from intracellular stores.

We could demonstrate that mAno6 existed in oocytes entirely as a non-covalently assembled homodimer, i.e., in the same oligomeric state as  $[\text{Ca}^{2+}]_i$ -activatable mAno1 [24]. A homodimeric stoichiometry of Ano6 has been reported previously by other authors [85]. The dimeric organization of the Ano family has been confirmed by X-ray crystallography of an Ano member from the fungus *Nectria haematococca* nHTMEM16 [12]. In view of the apparently correct assembly of Ano6, the lack of an increase in the  $\text{Cl}^-$  conductance secondary to the ATP activation of the co-expressed hP2X7R in oocytes of both *X. laevis* and Axolotl is surprising. We attribute this result, at least in part, to the weak expression of mAno6 in the plasma membrane. The EndoH sensitivity of most of the [ $^{35}\text{S}$ ]-methionine-labeled mAno6 strongly indicates that mAno6 is mostly retained in the endoplasmic reticulum of the oocytes, as has been previously observed with mammalian cells [21]. This is in stark contrast to the [ $^{35}\text{S}$ ]-methionine-labeled mAno1, which is completely converted into the complex-glycosylated form in oocytes.

Besides the weak plasma membrane expression, the need for long-term exposure to high  $\text{Ca}^{2+}$  levels in the 10–100- $\mu\text{M}$  range [32, 84] may have contributed to the observed lack of function of mAno6. These high  $\text{Ca}^{2+}$  levels may not be achieved in *X. laevis* oocytes through the application of A23187 or the ATP activation of hP2X7R. Notably, Ano6-mediated  $\text{Cl}^-$  currents could also not be activated by elevating intracellular  $\text{Ca}^{2+}$  levels in the various Ano6-overexpressing mammalian cell lines that exhibited high retention of Ano6 in the endoplasmic reticulum [21]. However, other authors found that activation of  $\text{Cl}^-$  currents in Ano6 expressing cells was possible via hypotonic stimuli [44].

**Benefits and limitations of *X. laevis* oocytes in studying P2 receptors and CaCCs** *X. laevis* oocytes are considered ideal for studying recombinant P2 receptors, as they do not endogenously express any functional P2 receptor [87]. This absence was also evident in the present study, in which absolutely no ATP-activatable ion currents were observed in either native oocytes or oocytes expressing mAno1 or mAno6 alone. In the analysis of GPCRs coupled to the  $\text{Ca}^{2+}$ -releasing  $\text{G}_q$  signaling pathway, such as P2Y1R and P2Y2R, the presence of oocyte-endogenous CaCCs [9, 91] has the distinct advantage of enabling easy electrophysiological monitoring of GPCR activation by TEVC. However, when recombinant CaCCs are studied, it must be considered that the oocyte-endogenous CaCC xAno1 mediates the predominant current in native oocytes [30, 50]. The detection of recombinantly expressed mAno1 against the background current mediated by xAno1 was nevertheless possible: secondary to the activation of recombinant mP2Y1R or hP2X7R, three- to fivefold larger CaCC currents were mediated by mAno1 than by oocyte-

endogenous xAno1. In addition, by conducting similar experiments in Axolotl oocytes, we verified that virtually the same results were obtained in the absence of any background of endogenously expressed CaCC(s).

An important implication of our study is that the secondary activation of endogenous CaCCs, particularly xAno1, must also be assumed to significantly contaminate the inward current recorded when recombinant P2X receptors are activated in *X. laevis* oocytes. P2X receptors exhibit considerable  $\text{Ca}^{2+}$  permeability, which is among the highest for all ligand-gated channels [22]. We believe that this secondary CaCC activation at least partly explains the slow increase in the macroscopic current observed during the long-lasting activation of hP2X7R by ATP or BzATP, which is usually attributed to pore dilation of P2X7R [56, 60]. Additionally, the reported P2X7R-related anion conductance [15, 20, 62, 67, 81] may actually be due to the secondary activation of anion channels, among which Ano1 is an obvious candidate. It has been shown that hP2X7R, itself, is not permeable to anions at either the whole-cell or single-channel level [10, 43].

**Similarities and dissimilarities in the activation of Ano1 via A23187, P2YR or P2X7R** Both the  $\text{Ca}^{2+}$  ionophore A23187 and ATP activation of the P2Y1R elicited relatively small transient currents through oocyte-endogenous xAno1 as well as exogenous mAno1. While the CaCC current secondary to P2Y1R activation is mechanistically limited by the limited  $\text{Ca}^{2+}$  available from intracellular stores, it would be expected that A23187 would evoke a significantly larger CaCC current by additionally mediating the uptake of extracellular  $\text{Ca}^{2+}$ . Because A23187 mediates the electrically neutral exchange of  $\text{Ca}^{2+}$  and other divalent cations for  $2\text{H}^+$  [23], the resulting increase in the intracellular pH may have an inhibitory effect on mAno1 activation. An alternative possibility is that the activation of Ano1 by increased  $[\text{Ca}^{2+}]_i$  is followed by its calmodulin-dependent inactivation, as observed in HEK293 cells in response to either A23187 or P2Y2R activation or the application of 1  $\mu\text{M}$   $\text{Ca}^{2+}$  through a whole-cell patch pipette [84]. If such inactivation also occurs in oocytes, it appears to play only a minor role when Ano1 is activated by the P2X7R-mediated  $\text{Ca}^{2+}$  influx.

Compared to the currents elicited via A23187 or P2Y2R activation, much larger, sustained CaCC currents were observed secondary to the ATP activation of hP2X7R. These differences in the sizes and shapes of the CaCC currents likely reflect differences in the speed, amplitude, and spatiotemporal propagation of the  $\text{Ca}^{2+}$  signals. Intracellular  $\text{Ca}^{2+}$  signals are substantially modulated by cytoplasmic  $\text{Ca}^{2+}$  buffers [77], and the mobility of  $\text{Ca}^{2+}$  in the cytosol of *X. laevis* oocytes is surprisingly slow [3]. Buffering and slow diffusion will primarily hinder  $\text{Ca}^{2+}$  released from the endoplasmic reticulum from reaching the  $\text{Ca}^{2+}$ -binding site of the CaCCs at the plasma membrane. In contrast,  $\text{Ca}^{2+}$  that enters the cell

through hP2X7R will have ready access to plasma membrane-bound CaCCs and will be subjected to less buffering, even if P2X7R and Ano1 are not in direct physical contact. Indeed, the kinetics of oocyte-endogenous CaCC currents have been found to be strongly correlated with submembranous  $\text{Ca}^{2+}$  levels [49]. Accordingly, the slow and fast activation of CaCC currents secondary to the activation of P2Y1R and hP2X7R, respectively, can be attributed to the existence of two  $\text{Ca}^{2+}$  subcompartments with slow and fast dynamics [49]. This attribution can likely also be applied to Ano1 activation in general.

**Possible physiological relevance of P2-Ano1 interactions** We consider the stimulation of Ano1 via P2Y and/or P2X7 receptors to be physiologically relevant. Exocrine glands often express CaCCs such as Ano1. The activation of P2Y and P2X7 receptors and secretion are both induced, at least in part, by extracellular ATP released from nerve endings or directly from epithelial cells [59]. In epithelial duct cells of the human pancreas, an organ that is severely affected in cystic fibrosis, both CFTR and Ano1  $\text{Cl}^-$  channels are subjected to purinergic regulation [89]. Of note, we could demonstrate in pancreatic cells the P2X7R-dependent activation of outwardly rectifying anion currents, which are most likely mediated by Ano1. A loss of Ano1 function has been found to impair mucus secretion in human airway surface epithelial cells and to reduce mucociliary clearance in the lung [36, 74]. Therefore, it is not only Ano1 activators that may be beneficial in the treatment of cystic fibrosis [54] but also activators of distinct P2 receptors. In P2X7-knockout mice, the sustained  $[\text{Ca}^{2+}]_i$  increase in the submandibular glands is nearly abolished, and secretion is concomitantly inhibited [53]. This result suggests that P2X7R activation plays an essential role in sustained secretion by secondarily activating CaCCs. P2X7R has been shown to be involved in secretion in rat lacrimal glands as well [35], which may also involve CaCCs.

**Possible role of the P2X7R-Ano1 connection in cancer** P2X7R is involved not only in inflammation and cell death but also in cell proliferation and carcinogenesis [1, 19]. Intriguingly, increasing lines of evidence further implicate Ano1 in cell proliferation and carcinogenesis: (i) Ano1 is highly expressed in gastrointestinal stromal tumors and regulates the proliferation of the interstitial cells of Cajal [80]; (ii) the selective Ano1 inhibitor T16Ainh-A01 reduces the proliferation of cultured Cajal cells and pancreatic cancer cells [51]; and (iii) the degree of overexpression of Ano1 in human prostate cancer tissues is correlated with the severity of disease, whereas the knockdown of Ano1 suppresses cell proliferation and metastasis in vitro and tumor growth in mice [47]. When both P2X7 and Ano1 are overexpressed in cancer cells, their functional interaction may have additive effects beyond the physiological regulation of cell proliferation. It will be

interesting to learn whether the combined inhibition of both targets exerts synergistic effects in suppressing the proliferation of cancer cells.

**Acknowledgments** We would like to thank the Deutsche Forschungsgemeinschaft (Ma1581/15-3; Schm536/9-3) for their financial support. We would also like to thank GlaxoSmithKline for their permission to use the monoclonal antibody against the hP2X7R ectodomain, Prof. Dr. Friedrich Koch-Nolte of University Medical Center, Hamburg for providing us with the corresponding hybridoma cell line, and Prof. Dr. Barbara Seliger, Institute for Medical Immunology of the Martin-Luther-University Halle for providing us the AsPC-1 cell line.

**Ethical standards** The experiments comply with the current laws of Germany.

## References

- Adinolfi E, Cirillo M, Woltersdorf R, Falzoni S, Chiozzi P, Pellegatti P, Callegari MG, Sandona D, Markwardt F, Schmalzing G, Di Virgilio F (2010) Trophic activity of a naturally occurring truncated isoform of the P2X7 receptor. *FASEB J* 24:3393–3404
- Adinolfi E, Pizzirani C, Idzko M, Panther E, Norgauer J, Di Virgilio F, Ferrari D (2005) P2X<sub>7</sub> receptor: death or life? *Purinergic Signal* 1: 219–227
- Allbritton NL, Meyer T, Stryer L (1992) Range of messenger action of calcium ion and inositol 1,4,5-trisphosphate. *Science* 258:1812–1815
- Alonso-Torre SR, Trautmann A (1993) Calcium responses elicited by nucleotides in macrophages—interaction between two receptor subtypes. *J Biol Chem* 268:18640–18647
- Amedee T, Despeyroux S (1995) ATP activates cationic and anionic conductances in Schwann cells cultured from dorsal root ganglia of the mouse. *Proc R Soc Lond B* 259:277–284
- Arreola J, Melvin JE (2003) A novel chloride conductance activated by extracellular ATP in mouse parotid acinar cells. *J Physiol Lond* 547:197–208
- Becker D, Woltersdorf R, Boldt W, Schmitz S, Braam U, Schmalzing G, Markwardt F (2008) The P2X<sub>7</sub> carboxyl tail is a regulatory module of P2X<sub>7</sub> receptor channel activity. *J Biol Chem* 283:25725–25734
- Boldt W, Klapperstück M, Büttner C, Sadtler S, Schmalzing N, Markwardt F (2003) Glu<sup>496</sup>Ala polymorphism of human P2X<sub>7</sub> receptor does not affect its electrophysiological phenotype. *Am J Physiol* 284:C749–C756
- Boton R, Dascal N, Gillo B, Lass Y (1989) Two calcium-activated chloride conductances in *Xenopus laevis* oocytes permeabilized with the ionophore A23187. *J Physiol Lond* 408:511–534
- Bretschneider F, Klapperstück M, Löhn M, Markwardt F (1995) Nonselective cationic currents elicited by extracellular ATP in human B-lymphocytes. *Pflugers Arch* 429:691–698
- Browne LE, Compan V, Bragg L, North RA (2013) P2X7 receptor channels allow direct permeation of nanometer-sized dyes. *J Neurosci* 33:3557–3566
- Brunner JD, Lim NK, Schenck S, Duerst A, Dutzler R (2014) X-ray structure of a calcium-activated TMEM16 lipid scramblase. *Nature* 516:207–212
- Buell G, Chessell IP, Michel AD, Colo G, Salazzo M, Herren S, Gretener D, Grahames C, Kaur R, Kosco-Vilbois MH, Humphrey PPA (1998) Blockade of human P2X<sub>7</sub> receptor function with a monoclonal antibody. *Blood* 92:3521–3528

14. Caputo A, Caci E, Ferrera L, Pedemonte N, Barsanti C, Sondo E, Pfeffer U, Ravazzolo R, Zegarra-Moran O, Galiotta LJ (2008) TMEM16A, a membrane protein associated with calcium-dependent chloride channel activity. *Science* 322:590–594
15. Cervetto C, Alloisio S, Frattaroli D, Mazzotta MC, Milanese M, Gavazzo P, Passalacqua M, Nobile M, Maura G, Marcoli M (2013) The P2X7 receptor as a route for non-exocytotic glutamate release: dependence on the carboxyl tail. *J Neurochem* 124:821–831
16. Colomar A, Amedee T (2001) ATP stimulation of P2X<sub>7</sub> receptors activates three different ionic conductances on cultured mouse Schwann cells. *Eur J Neurosci* 14:927–936
17. Detro-Dassen S, Schanzler M, Lauks H, Martin I, zu Berstenhorst SM, Nothmann D, Torres-Salazar D, Hidalgo P, Schmalzing G, Fahlke C (2008) Conserved dimeric subunit stoichiometry of SLC26 multifunctional anion exchangers. *J Biol Chem* 283:4177–4188
18. Di Virgilio F (2007) Liaisons dangereuses: P2X<sub>7</sub> and the inflammasome. *Trends Pharmacol Sci* 28:465–472
19. Di Virgilio F, Ferrari D, Adinolfi E (2009) P2X<sub>7</sub>: a growth-promoting receptor-implications for cancer. *Purinergic Signal* 5:251–256
20. Duan SM, Anderson CM, Keung EC, Chen YM, Chen YR, Swanson RA (2003) P2X<sub>7</sub> receptor-mediated release of excitatory amino acids from astrocytes. *J Neurosci* 23:1320–1328
21. Duran C, Qu Z, Osunkoya AO, Cui Y, Hartzell HC (2012) ANOs 3–7 in the anoctamin/mem16 Cl<sup>-</sup> channel family are intracellular proteins. *Am J Physiol* 302:C482–C493
22. Egan TM, Khakh BS (2004) Contribution of calcium ions to P2X channel responses. *J Neurosci* 24:3413–3420
23. Erdahl WL, Chapman CJ, Taylor RW, Pfeiffer DR (1994) Ca<sup>2+</sup> transport properties of ionophores A23187, ionomycin, and 4-BrA23187 in a well defined model system. *Biophys J* 66:1678–1693
24. Fallah G, Römer T, Braam U, Detro-Dassen S, Markwardt F, Schmalzing G (2011) TMEM16A(a)/anoctamin-1 shares a homodimeric architecture with CLC chloride channels. *Mol Cell Proteomics*. doi:10.1074/mcp.M110.004697
25. Faria RX, Reis R, Casabulho CM, Alberto AP, Fernando DP, Henriques-Pons A, Alves LA (2009) Pharmacological properties of a pore induced by raising intracellular Ca<sup>2+</sup>. *Am J Physiol* 297:C28–C42
26. Flittiger B, Klapperstück M, Schmalzing G, Markwardt F (2010) Effects of protons on macroscopic and single-channel currents mediated by the human P2X<sub>7</sub> receptor. *Biochim Biophys Acta Biomembranes* 1798:947–957
27. Galiotta LJV (2009) The TMEM16 protein family: a new class of chloride channels? *Biophys J* 97:3047–3053
28. Gendreau S, Voswinkel S, Torres-Salazar D, Lang N, Heidtmann H, Detro-Dassen S, Schmalzing G, Hidalgo P, Fahlke C (2004) A trimeric quaternary structure is conserved in bacterial and human glutamate transporters. *J Biol Chem* 279:39505–39512
29. Gloor S, Pongs O, Schmalzing G (1995) A vector for the synthesis of cRNAs encoding Myc epitope-tagged proteins in *Xenopus laevis* oocytes. *Gene* 160:213–217
30. Gomez-Hernandez JM, Stühmer W, Parekh AB (1997) Calcium dependence and distribution of calcium-activated chloride channels in *Xenopus* oocytes. *J Physiol Lond* 502:569–574
31. Griffon N, Buttner C, Nicke A, Kuhse J, Schmalzing G, Betz H (1999) Molecular determinants of glycine receptor subunit assembly. *EMBO J* 18:4711–4721
32. Grubb S, Poulsen KA, Juul CA, Kyed T, Klausen TK, Larsen EH, Hoffmann EK (2013) TMEM16F (Anoctamin 6), an anion channel of delayed Ca<sup>2+</sup> activation. *J Gen Physiol* 141:585–600
33. Grudzien-Nogalska E, Stepinski J, Jemielity J, Zuberek J, Stolarski R, Rhoads RE, Darzynkiewicz E (2007) Synthesis of anti-reverse cap analogs (ARCA)s and their applications in mRNA translation and stability. *Methods Enzymol* 431:203–227
34. Haeger S, Kuzmin D, Detro-Dassen S, Lang N, Kilb M, Tsetlin V, Betz H, Laube B, Schmalzing G (2010) An intramembrane aromatic network determines pentameric assembly of Cys-loop receptors. *Nat Struct Mol Biol* 17:90–98
35. Hodges RR, Vrouvlianis J, Shatos MA, Dartt DA (2009) Characterization of P2X7 purinergic receptors and their function in rat lacrimal gland. *Invest Ophthalmol Vis Sci* 50:5681–5689
36. Huang F, Zhang H, Wu M, Yang H, Kudo M, Peters CJ, Woodruff PG, Solberg OD, Donne ML, Huang X, Sheppard D, Fahy JV, Wolters PJ, Hogan BL, Finkbeiner WE, Li M, Jan YN, Jan LY, Rock JR (2012) Calcium-activated chloride channel TMEM16A modulates mucin secretion and airway smooth muscle contraction. *Proc Natl Acad Sci U S A* 109:16354–16359
37. Hung AC, Chu YJ, Lin YH, Weng JY, Chen HB, Au YC, Sun SH (2005) Roles of protein kinase C in regulation of P2X<sub>7</sub> receptor-mediated calcium signalling of cultured type-2 astrocyte cell line, RBA-2. *Cell Signal* 17:1384–1396
38. Kim M, Jiang LH, Wilson HL, North RA, Surprenant A (2001) Proteomic and functional evidence for a P2X<sub>7</sub> receptor signalling complex. *EMBO J* 20:6347–6358
39. King BF, Townsend-Nicholson A (2003) Nucleotide and nucleoside receptors. *Toxicol Rev* 23:1–11
40. Klapperstück M, Büttner C, Böhm T, Schmalzing G, Markwardt F (2000) Characteristics of P2X<sub>7</sub> receptors from human B lymphocytes expressed in *Xenopus* oocytes. *Biochim Biophys Acta* 1467:444–456
41. Klapperstück M, Büttner C, Schmalzing G, Markwardt F (2001) Functional evidence of distinct ATP activation sites at the human P2X<sub>7</sub> receptor. *J Physiol Lond* 534:25–35
42. Kmit A, van Krachten R, Ousingsawat J, Mattheij NJ, Senden-Gijsbers B, Heemskerk JWM, Schreiber R, Bevers EM, Kunzelmann K (2013) Calcium-activated and apoptotic phospholipid scrambling induced by Ano6 can occur independently of Ano6 ion currents. *Cell Death Dis* 4:e611
43. Kubick C, Schmalzing G, Markwardt F (2011) The effect of anions on the human P2X7 receptor. *Biochim Biophys Acta Biomembranes* 1808:2913–2922
44. Kunzelmann K, Nilius B, Owsianik G, Schreiber R, Ousingsawat J, Sirian L, Wanitchakool P, Bevers EM, Heemskerk JWM (2013) Molecular functions of anoctamin 6 (TMEM16F): a chloride channel, cation channel, or phospholipid scramblase? *Pflugers Arch* 466: 407–414
45. Kunzelmann K, Tian Y, Martins JR, Faria D, Kongsuphol P, Ousingsawat J, Thevenod F, Roussa E, Rock J, Schreiber R (2011) Anoctamins. *Pflugers Arch* 426:195–208
46. Kuruma A, Hartzell HC (1999) Dynamics of calcium regulation of chloride currents in *Xenopus* oocytes. *Am J Physiol* 276:C161–C175
47. Liu W, Lu M, Liu B, Huang Y, Wang K (2012) Inhibition of Ca<sup>2+</sup>-activated Cl<sup>-</sup> channel ANO1/TMEM16A expression suppresses tumor growth and invasiveness in human prostate carcinoma. *Cancer Lett* 326:41–51
48. Löhn M, Klapperstück M, Riemann D, Markwardt F (2001) Sodium block and depolarization diminish P2Z-dependent Ca<sup>2+</sup> entry in human B lymphocytes. *Cell Calcium* 29:395–408
49. Machaca K, Hartzell HC (1999) Reversible Ca gradients between the subplasmalemma and cytosol differentially activate Ca-dependent Cl currents. *J Gen Physiol* 113:249–266
50. Machaca K, Qu Z, Kuruma A, Hartzell HC, McCarty N (2002) The endogenous Ca-activated Cl channel in *Xenopus* oocytes: a physiologically and biophysical rich model system. *Curr Top Membr* 53:3–39
51. Mazzone A, Eisenman ST, Strege PR, Yao Z, Ordog T, Gibbons SJ, Farrugia G (2012) Inhibition of cell proliferation by a selective inhibitor of the Ca<sup>2+</sup>-activated Cl<sup>-</sup> channel, Ano1. *Biochem Biophys Res Commun* 427:248–253
52. Mehta VB, Hart J, Hewers MD (2001) ATP-stimulated release of interleukin (IL)-1β and IL-18 requires priming by lipopolysaccharide

- and is independent of caspase-1 cleavage. *J Biol Chem* 276:3820–3826
53. Nakamoto T, Brown DA, Catalan MA, Gonzalez-Begne M, Romanenko VG, Melvin JE (2009) Purinergic P2X<sub>7</sub> receptors mediate ATP-induced saliva secretion by the mouse submandibular gland. *J Biol Chem* 284:4815–4822
54. Namkung W, Yao Z, Finkbeiner WE, Verkman AS (2011) Small-molecule activators of TMEM16A, a calcium-activated chloride channel, stimulate epithelial chloride secretion and intestinal contraction. *FASEB J* 25:4048–4062
55. Nicke A, Bäumert HG, Rettiger J, Eichele A, Lambrecht G, Mutschler E, Schmalzing G (1998) P2X<sub>1</sub> and P2X<sub>3</sub> receptors form stable trimers: a novel structural motif of ligand-gated ion channels. *EMBO J* 17:3016–3028
56. Nicke A, Kuan YH, Masin M, Rettiger J, Marquez-Klaka B, Bender O, Gorecki DC, Murrell-Lagnado RD, Soto F (2009) A functional P2X<sub>7</sub> splice variant with an alternative transmembrane domain 1 escapes gene inactivation in P2X<sub>7</sub> KO mice. *J Biol Chem* 284: 25813–25822
57. Nicke A, Thurau H, Sadtler S, Rettiger J, Schmalzing G (2004) Assembly of nicotinic  $\alpha$ 7 subunits in *Xenopus* oocytes is partially blocked at the tetramer level. *FEBS Lett* 575:52–58
58. North RA (2002) Molecular physiology of P2X receptors. *Physiol Rev* 82:1013–1067
59. Novak I (2011) Purinergic signalling in epithelial ion transport—regulation of secretion and absorption. *Acta Physiol (Oxf)* 202:501–522
60. Paukert M, Hidayat S, Gründer S (2002) The P2X<sub>7</sub> receptor from *Xenopus laevis*: formation of a large pore in *Xenopus* oocytes. *FEBS Lett* 513:253–258
61. Pelegri P, Surprenant A (2006) Pannexin-1 mediates large pore formation and interleukin-1 release by the ATP-gated P2X<sub>7</sub> receptor. *EMBO J* 25:5071–5082
62. Pellegatti P, Falzoni S, Pinton P, Rizzuto R, Di Virgilio F (2005) A novel recombinant plasma membrane-targeted luciferase reveals a new pathway for ATP secretion. *Mol Biol Cell* 16:3659–3665
63. Rais I, Karas M, Schagger H (2004) Two-dimensional electrophoresis for the isolation of integral membrane proteins and mass spectrometric identification. *Proteomics* 4:2567–2571
64. Ralevic V, Burnstock G (1998) Receptors for purines and pyrimidines. *Pharmacol Rev* 50:413–492
65. Rassendren F, Buell GN, Virginio C, Collo G, North RA, Surprenant A (1997) The permeabilizing ATP receptor, P2X<sub>7</sub>—cloning and expression of a human cDNA. *J Biol Chem* 272:5482–5486
66. Rath A, Deber CM (2013) Correction factors for membrane protein molecular weight readouts on sodium dodecyl sulfate-polyacrylamide gel electrophoresis. *Anal Biochem* 434:67–72
67. Reyes JP, Perez-Cornejo P, Hernandez-Carballo CY, Srivastava A, Romanenko VG, Gonzalez-Begne M, Melvin JE, Arreola J (2008) Na<sup>+</sup> modulates anion permeation and blocks of P2X<sub>7</sub> receptors from mouse parotid glands. *J Membr Biol* 223:73–85
68. Riedel T, Lozinsky I, Schmalzing G, Markwardt F (2007) Kinetics of P2X<sub>7</sub> receptor-operated single channels currents. *Biophys J* 92:2377–2391
69. Riedel T, Schmalzing G, Markwardt F (2007) Influence of extracellular monovalent cations on pore and gating properties of P2X<sub>7</sub> receptor-operated single channels currents. *Biophys J* 93:846–858
70. Saiyed T, Paarmann I, Schmitt B, Haeger S, Sola M, Schmalzing G, Weissenhorn W, Betz H (2007) Molecular basis of gephyrin clustering at inhibitory synapses: role of G- and E-domain interactions. *J Biol Chem* 282:5625–5632
71. Sauter DR, Novak I, Pedersen SF, Larsen EH, Hoffmann EK (2014) ANO1 (TMEM16A) in pancreatic ductal adenocarcinoma (PDAC). *Pflugers Arch.* doi:10.1007/s00424-014-1598-8:
72. Schmalzing G, Kröner S, Schachner M, Gloer S (1992) The adhesion molecule on glia (AMOG/beta 2) and alpha 1 subunits assemble to functional sodium pumps in *Xenopus* oocytes. *J Biol Chem* 267: 20212–20216
73. Schmalzing G, Ruhl K, Gloer SM (1997) Isoform-specific interactions of Na<sup>+</sup>, K<sup>+</sup>-ATPase subunits are mediated via extracellular domains and carbohydrates. *Proc Natl Acad Sci U S A* 94:1136–1141
74. Schreiber R, Ulyakina I, Kongsuphol P, Warth R, Mirza M, Martins JR, Kunzelmann K (2010) Expression and function of epithelial anoctamins. *J Biol Chem* 285:7838–7845
75. Schroeder BC, Cheng T, Jan YN, Jan LY (2008) Expression cloning of TMEM16A as a calcium-activated chloride channel subunit. *Cell* 134:1019–1029
76. Schubert R (1996) Multiple ligand-ion solutions: a guide for solution preparation and computer program understanding. *J Vasc Res* 33:86–98
77. Schwaller B (2010) Cytosolic Ca<sup>2+</sup> buffers. *Cold Spring Harb Perspect Biol* 2:a004051
78. Shimizu T, Ichara T, Sato K, Fujii T, Sakai H, Okada Y (2013) TMEM16F is a component of a Ca<sup>2+</sup>-activated Cl<sup>−</sup> channel but not a volume-sensitive outwardly rectifying Cl<sup>−</sup> channel. *Am J Physiol* 304:C748–C759
79. Solini A, Chiozzi P, Morelli A, Fellin R, Di Virgilio F (1999) Human primary fibroblasts in vitro express a purinergic P2X<sub>7</sub> receptor counted to ion fluxes, microvesicle formation and IL-6 release. *J Cell Sci* 112:297–305
80. Stanich JE, Gibbons SJ, Eisenman ST, Bardsley MR, Rock JR, Harfe BD, Ordog T, Farrugia G (2011) ANO1 as a regulator of proliferation. *Am J Physiol* 301:G1044–G1051
81. Suadicani SO, Brosnan CF, Scemes E (2006) P2X<sub>7</sub> receptors mediate ATP release and amplification of astrocytic intercellular Ca<sup>2+</sup> signaling. *J Neurosci* 26:1378–1385
82. Suzuki J, Umehara M, Sims PJ, Nagata S (2010) Calcium-dependent phospholipid scrambling by TMEM16F. *Nature* 468:834–838
83. Takahashi T, Neher E, Sakmann B (1987) Rat brain serotonin receptors in *Xenopus* oocytes are coupled by intracellular calcium to endogenous channels. *Proc Natl Acad Sci U S A* 84:5063–5067
84. Tian Y, Schreiber R, Kunzelmann K (2012) Anoctamins are a family of Ca<sup>2+</sup>-activated Cl<sup>−</sup> channels. *J Cell Sci* 125:4991–4998
85. Tien J, Lee HY, Minor DL Jr, Jan YN, Jan LY (2013) Identification of a dimerization domain in the TMEM16A calcium-activated chloride channel (CaCC). *Proc Natl Acad Sci U S A* 110:6352–6357
86. Tokuyama Y, Hara M, Jones EM, Fan Z, Bell GI (1995) Cloning of rat and mouse P2Y purinoceptors. *Biochem Biophys Res Commun* 211:211–218
87. Valera S, Hussy N, Evans RJ, Adami N, North RA, Surprenant A, Buell G (1994) A new class of ligand-gated ion channel defined by P2x receptor for extracellular ATP. *Nature* 371:516–519
88. von Känelgen I (2006) Pharmacological profiles of cloned mammalian P2Y-receptor subtypes. *Pharmacol Ther* 110:415–432
89. Wang J, Haanes KA, Novak I (2013) Purinergic regulation of CFTR and Ca<sup>2+</sup>-activated Cl<sup>−</sup> channels and K<sup>+</sup> channels in human pancreatic duct epithelium. *Am J Physiol* 304:C673–C684
90. Weber W (1999) Ion currents of *Xenopus laevis* oocytes: state of the art. *Biochim Biophys Acta* 1421:213–233
91. Weber WM (1999) Endogenous ion channels in oocytes of *xenopus laevis*: recent developments. *J Membr Biol* 170:1–12
92. Wilson HL, Wilson SA, Surprenant A, North RA (2002) Epithelial membrane proteins induce membrane blebbing and interact with the P2X<sub>7</sub> receptor C terminus. *J Biol Chem* 277:34017–34023
93. Yang YD, Cho H, Koo JY, Tak MH, Cho Y, Shim WS, Park SP, Lee J, Lee B, Kim BM, Raouf R, Shin YK, Oh U (2008) TMEM16A confers receptor-activated calcium-dependent chloride conductance. *Nature* 455:1210–1215